C. Olla, P. C. Ricci, D. Chiriu, M. Fantauzzi, M. F. Casula, F. Mocci, A. Cappai, S. Porcu, L. Stagi, C. M. Carbonaro

Selecting molecular or surface centers in Carbon Dots-silica hybrids to tune the optical emission: a photo-physics study down to the atomistic level

Journal of Colloid and Interface Science, 634 (2023) 402–417

Selecting molecular or surface centers in Carbon Dots-silica hybrids to tune the optical emission: a photo-physics study down to the atomistic level

Chiara Olla, Pier Carlo Ricci, Daniele Chiriu, Marzia Fantauzzi, Maria Francesca Casula, Francesca Mocci, Antonio Cappai, Stefania Porcu, Luigi Stagi, Carlo Maria Carbonaro**

C. Olla, P.C. Ricci, D. Chiriu, A. Cappai, S. Porcu, C.M. Carbonaro
Department of Physics,
University of Cagliari, I-09042 Monserrato, Italy
E-mail: chiara.olla@dsf.unica.it, cm.carbonaro@dsf.unica.it
M. Fantauzzi, F. Mocci
Department of Chemical and Geological Sciences,
University of Cagliari, I-09042 Monserrato, Italy
M.F. Casula
Department of Mechanical, Chemical, and Materials Engineering,
University of Cagliari, Via Marengo 2, IT 09123 Cagliari, Italy
L. Stagi
Department of Chemistry and Pharmacy,
Laboratory of Materials Science and Nanotechnology,
University of Sassari, via Vienna 2, 07100 Sassari, Italy

Keywords:
Carbon dots, green fluorescence properties, emission mechanism, silica hybrids, silica matrices, photo-physics

In this work, we unveil the fluorescence features of citric acid and urea-based Carbon Dots (CDs) through a photo-physical characterization of nanoparticles synthesized, under solvent-free and open-air conditions, within silica-ordered mesoporous silica, as a potential host for solid-state emitting hybrids. Compared to CDs synthesized without silica matrices and dispersed in water, silica-CD hybrids display a broader emission in the green range whose contribution can be increased by UV and blue laser irradiation. The analysis of hybrids synthesized within different silica (MCM-48 and SBA-15) calls for an active role of the matrix in directing the synthesis toward the formation of CDs with a larger content of graphitic N and imidic groups at the expense of N-pyridinic molecules. As a result, CDs tuned in size and with

a larger green emission are obtained both in the hybrids and once extracted from the silica matrix and dispersed in water. The kinetics of the photo-physics under UV and blue irradiation of hybrid samples show a photo-assisted formation process leading to a further increase of the relative contribution of the green emission, not observed in the water-dispersed reference samples, suggesting that the porous matrix is involved also in the photo-activated process. Finally, we carried out DFT and TD-DFT calculations on the interaction of silica with selected models of CD emitting centers, like surface functional groups (OH and COOH), dopants (graphitic N), and citric acid-based molecules. The combined experimental and theoretical results clearly indicate the presence of molecular species and surface centers both emitting in the blue and green spectral range, whose relative contribution is tuned by the interaction with the surrounding media.

1. Introduction

Over the past few years, a big effort has been made to replace semiconductor quantum dots and rare-earth-based materials currently adopted in optoelectronics and photonics with more environmental-friendly and cost-effective fluorophores. A promising green and low-cost alternative is represented by a wide class of fluorescent carbon-based nanoparticles known as Carbon Dots (CDs). Indeed, CD's high quantum yield (QY) in the blue-green wavelength region can reach values comparable to their inorganic counterparts, with limitations in the red range that can be partially overcome by proper functionalization of the surface[1–3] or *ad-hoc* doping[4,5].

CD's main feature is their almost ubiquitous excitation dependence on tunable and efficient photoluminescence, the emission properties being easily modified by chemical functionalization and surface passivation[6–8]. These optical properties, along with high chemical inertness, resistance to photobleaching, and biocompatibility, make them highly desirable not only to produce lighting devices but also for biomedicine and drug delivery purposes[9–12]. In addition, the interaction with selected host matrices further spread the applications from sensing to optoelectronics[13–15].

Despite all these advantages, CDs present some critical issues to deal with to develop CD-based technology. The main question concerns the lack of deep knowledge about their structure which is strongly linked to the origin of their photoluminescence. At present, their emission properties are not exclusively ascribed to a single mechanism: quantum confinement, due to their hypothesized nanosized sp^2 carbon core, and molecular states or surface states, due to

fluorophores formation and surface traps, respectively, are both considered[16,17]. Also, the synergic interplay between the proposed models is an important aspect[18], further complicating the scenario. Indeed, the observation of more than one emission band along with their typical broad width, and the excitation dependence mentioned above, call for a specific distribution of centers, and potentially multiple emission mechanisms are required to account for the overall picture. At the present state of the art, since structural and optical features of CDs largely depend on synthetic conditions such as temperature, pressure, and precursors[19–21], a clear correlation between composition, structure, and chemical-physical properties has not been established.

CD production generally involves the pyrolysis or carbonization of small organic molecules, that build complex systems with predicted molecular features, as largely assessed by previous studies[20,22–24]. The formation of polyaromatic hydrocarbons (PAHs) within the core structure or as sp^2 surface islands is expected[25–27]. Thermal degradation of citric acid, one of the most suitable CD precursors, produces, by itself, a few fluorescent compounds which are supposed to be involved in the luminescent properties of citrate-based systems[28] whilst the addition of nitrogen sources, such as urea as in the present case, are reported to enhance the QY [29–31] and to produce fluorescent molecules like citrazinic acid (CZA), its derivatives, [24,32–35] or other efficient blue and green emitting molecules, such as 1,2,3,5-tetrahydro-5-oxo-imidazo[1,2-a]pyridine-7-carboxylic acid (known as IPCA)[36] or 4-hydroxy-1H-pyrrolo[3,4-c]pyridine-1,3,6(2H,5H)-trione (known as HPPT)[37]. It was recently shown that these molecules can be also embedded within the CD structure, also forming aggregated structures acting as a seed for CD nucleation and producing nanosized graphitic-like domains[38–40]. Besides fluorescent molecules, surface functional groups, like OH, COOH or NH_2, cause emission features in the blue-green region[6,41–43], as well as the introduction of graphitic N[42,44].

The large panorama of possible emitting centers further pinpoints the need to determine the connection between CD structure and emission mechanism, also in view of proper exploitation of the resulting properties for the desired application[12,45]. To achieve this goal, a larger control on the obtained synthesis products, in terms of structure, composition, and morphology, possibly through a fast, easy, and green synthesis procedure, is required. Bottom-up routes represent an efficient method to obtain CDs in a cheaper way on large scale but make it difficult to achieve homogenous samples in size and distribution, thus requiring complex purification procedures. A valid approach consists of the production of CDs directly in porous solid-state matrices using them as nanoreactors to obtain size-selected nanoparticles[46,47]. Host matrices

such as polymers[48–51], zeolites[52,53], MOFs[54], silica gel[55–58], and different mesoporous materials[59–61] provide multipotential support for the production of hybrid fluorescent materials for several purposes including room temperature phosphorescence and delayed fluorescence applications[62–64].

Recently, we studied similar hybrid systems obtained by imbibition of mesoporous silica matrices with citrate-based CDs and focused on the optical emission change due to the interaction with the matrix[8,65]. The use of mesoporous silica as a suitable solid-state matrix for CDs is motivated, among others, by its well-known chemical inertness and high specific surface[66,67]. In this work, we investigate the properties of CDs synthesized within solid-state matrices of commercially available mesoporous silica employing a solvent-free synthesis in an open-air oven and comparing the photophysical properties of solid-state hybrids with those of reference CDs prepared without silica matrices and dispersed in water (CD-R). Using as precursors citric acid (CA) and urea, we synthesized CDs directly inside two types of mesoporous silica with different morphologies and pore sizes (commercial MCM-48, with 3 nm pore diameter, and SBA-15, with 8 nm pore diameter, S3, and S8 respectively in the following). The aim is to investigate a solvent-free solid-state synthesis[68], exploiting silica matrices as nanoreactors to produce homogeneous CDs, avoiding complicated separation and purification procedures. Optical and structural properties of solid-state hybrids (S-CD) were measured and compared to the ones of CD-R by means of a multi-technique approach, encompassing irradiation-driven photophysics experiments and quantum chemistry simulations to verify which could be the possible emitting centers in the blue and green region and why the green ones are promoted when CDs are synthesized within silica matrix. Finally, we verified that those optical properties tuned by the synthesis within mesoporous silica were also preserved once the CDs (CD-E) were extracted from the host matrices.

2. Experimental and Computational details

2.1. Synthesis and Treatments

Reference nitrogen-doped CDs (CD-R) were synthesized via simple thermal decomposition of precursors in air and represent our reference sample. A 1:1 mol mixture of citric acid (1 g) and urea (0.285 g), all purchased from Sigma Aldrich, were dissolved in 10 mL of distilled water and stirred in an ultrasonic bath for 15 minutes. Afterward, 2 mL of solution was transferred, put in a drying oven at 80 °C until the complete evaporation of water (in this sense the synthesis is defined as solvent-free), and heated in an open vessel at 180 °C for 3 hours. The upward ramp was set to 10 °C/min starting from room temperature (RT) and, at the end of the

cycle, the sample was slowly cooled down since it reached RT again. Finally, we dissolved the produced powder in 40 mL of water and separated larger aggregates utilizing a centrifuge (30 min at 6000 rpm).

The synthesis of CDs directly in a matrix of mesoporous silica spheres (S-CD) was performed by drop casting the same aqueous solution of citric acid and urea upon mesoporous silica powders (MCM-48 and SBA-15, Sigma Aldrich) with different pore sizes (3 nm and 8 nm in diameter, as declared by the producer). Impregnated powders were left in a drying oven at 80 °C for about 45 minutes, allowing water to slowly evaporate (again solvent-free synthesis, water was exploited as a vector to introduce the precursors within the silica matrices), and finally put in the oven at 180 °C for 3 hours, as previously described. After cooling down the hybrid samples, S3-CD and S8-CD were ready for measurements.

We also prepared silica samples soaked with the pre-formed reference CDs dispersed in water (I-CD) to compare the irradiation effects on different hybrid samples. Soaking was obtained by drop-casting 1 ml of CD water dispersion on 7 mg of bare silica powders.

To extract the CDs synthesized in silica matrices we performed a series of washing treatments in water, filtering the washed powders (filter pore size 0.22 μm) and collecting the water solution with the extracted CDs (CD-E)

2.2. Measurements and calculations

2.2.1. Structural, textural and morphological characterization

Transmission electron microscopy (TEM) images were acquired with a Jeol JEM 1400 Plus microscope. Once dispersed in a tiny amount of n-octane the samples were dropcasted on a holey carbon-coated copper grid and let evaporate at RT.

Infrared spectra were collected by using a Bruker Vertex 70 spectrometer in the range 4000–400 cm^{-1} with a resolution of 4 cm^{-1} and 256 scans, using KBr pellets. Spectra were acquired in absorbance mode to measure the attenuated total reflection (ATR) of powders and dispersed samples.

XPS analysis was performed with a Theta Probe ARXPS spectrometer (Thermo Fischer Scientific) using the AlKα source at 70 W. The analyzer was operated in the fixed analyzer transmission mode. Three points with a spot size of 300 μm were analyzed on each sample. The residual pressure in the UHV chamber was always lower than 5×10^{-7} Pa. The binding energy scale was calibrated using the standard procedure. Sample charging was compensated by referring all binding energies to the C_{1s} signal at 285 eV. More details on experimental setup and data processing are provided by Fermo et al[69].

N_2 physisorption experiments at 77 K were performed using a Sorptomatic 1990 System (Fisons Instrument). Prior to measurements, the samples were outgassed at room temperature for 24 hours.

2.2.2. Steady-state and Time-resolved optical spectroscopy

UV-Vis-NIR absorbance and reflectance spectra were collected by an Agilent Cary 5000 spectrophotometer with a spectral bandwidth of 2 nm in the 200-800 nm range. All the liquid samples were diluted with distilled water and put in quartz cuvettes with a 1 cm path length. Baseline corrections were performed on all spectra.

Three-dimensional fluorescence maps were performed using a spectrofluorometer Horiba Jobin Yvon Fluoromax-3 with a 450 W xenon lamp as the excitation source. The maps were collected with an excitation range of 300-600 nm and an emission range of 300-600 nm with a 2 nm slit for excitation and emission.

QY measurements for hybrid solid samples were carried out by comparing the light emitted by the samples to a reference dye excited at 350 nm, as described in [8,70], according to the following expression:

$$QY = QY_R \frac{I\, OD_R n^2}{I_R OD n_R^2}$$

where the subscript *R* refers to the reference (C120), *I* is the PL intensity of the sample, *OD* indicates the optical density evaluated at the excitation wavelength, and *n* refers to the refractive index of the relative solvent.

In the case of samples dispersed in water, QY measurements were performed by means of an integrating sphere paired with a Jasco FP-8550 spectrofluorometer at 350 and 440 nm excitation wavelengths.

As for time-resolved photoluminescence (TR-PL), the measurements were performed by exciting the samples with 200 fs long pulses delivered by an optical parametric amplifier (Light Conversion TOPAS-C) pumped by a regenerative Ti:Sapphire amplifier (Coherent Libra-HE). The repetition frequency was 1 kHz, and the PL signal was recovered by a streak camera (Hamamatsu C10910) equipped with a grating spectrometer (Princeton Instruments Acton SpectraPro SP-2300). All the TR-PL measurements were gathered by exciting the samples in the front-face mode to avoid the inner filter effect. In the case of CDs dispersed in water the solutions were placed in quartz cuvettes with a 1 cm path length. Solid hybrids were placed between transparent glass slides. Proper optical filters were applied when needed.

2.2.3. DFT and TD-DFT calculations

Quantum-chemistry calculations were performed using the Gaussian 16 suite of programs [71]. To model the silica matrix, we considered a cluster of 14 silicon atoms previously reported[72,73]. H or OH atoms terminated the dangling bonds of the surface Si atoms in the clusters. As for the representative emitting centers in CDs we considered different possible models: two selected molecules, the keto tautomer of CZA and HPPT molecules, which, from preliminary calculations, were more stable in water solution than the imine tautomer[40,74]; the OH and COOH functional groups at the edge of a pyrene structure (an archetypal PAH system to mimic carbon network of CDs[75]) and, finally, the presence of graphitic N within the same reference pyrene structure.

We performed a geometry optimization down to the self-consistent field (SCF) energy of each model system by means of DFT calculations carried out at the B3LYP/6-311++G(d,p) theory level[76,77]. Vibrational analysis on each optimized structure was performed to verify the absence of imaginary frequencies (the structures correspond to true local minima).

No solvent effect was accounted for since no water is supposed to be present within the silica mesoporous matrix after CD synthesis. However, to consider the possibility of some residual OH group at the silica surface some calculations were carried out by substituting the terminal H atoms of the silica cluster with 1 to 4 OH groups on the selected interaction sites with model structures. We also tested the system with full OH coverage.

To evaluate the silica-CD interaction we performed rigid scan calculations to probe the potential energy surface (PES) along a specific interaction coordinate and selected a few possible trajectories and interaction sites. Both the silica cluster model and the CD models were kept at frozen optimized positions during the scan (rigid scan procedure) to reduce the freedom degrees of the system. Once a minimum of energy in the PES was individuated, we performed TD-DFT/B3LYP/6-31G(d) and 6-311++G(d,p) calculations of that structure to calculate UV-VIS optical absorption. We also let the system relax from the fixed position minimum and re-calculated the UV-VIS features in the relaxed geometry at the same theory level.

3. Results and Discussion

3.1 Optical and structural characterization

The absorption spectrum (**Figure 1**a) of the reference CD dispersed in water (CD-R) and synthesized through the solvent-free approach here proposed reproduces the typical bands reported for citric-acid derived CDs, with a distinct contribution peaked at about 345 nm usually ascribed to n-π* transitions and a far UV band related to π-π* ones. Besides, a shoulder around 375 nm and a broad band at about 440 nm are also detected. When CD synthesis is performed

within mesoporous silica and the solid-state samples are analyzed (S-CD), the relative contribution of the broad absorption band above 375 nm is largely increased compared to the main one at 350 nm recorded in CD-R dispersed in water. The gathered spectra suggest that the small shoulders peaked at about 375 and 440 nm observed in CDs in water keep their peak position and are largely increased in the hybrid samples. In addition, the S8-CD hybrid 350 nm absorption band is still resolved and larger than the broad shoulder in the blue range, whilst S3-CD near-UV band is not distinct anymore, its relative content being even lower than the blue one. These findings indicate that we should expect in hybrid samples an increase in the contribution of the emitting centers related to the absorption in the 375-450 nm range, in good agreement with our previous results[8].

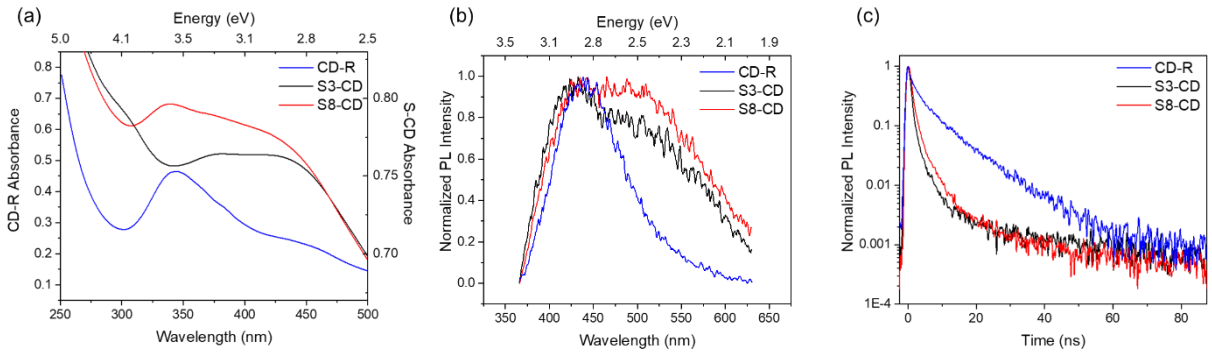

Figure 1. (a) Absorbance spectrum of CD-R and S-CD hybrids, (b) comparison of TR-PL spectra excited at 350 nm with an excitation power of 2.5 μW, (c) and the relative decay time plots in the 100 ns range.

Comparing the emission features of hybrid samples to the ones of CD-R at 350 nm excitation wavelength and low laser power (2.5 μW), we indeed confirm a larger relative contribution of the green emission band (**Figure 1**b), paired with an overall reduced lifetime because of the interaction with the silica matrix and possible aggregation phenomena within the porous host (**Figure 1**c). The detailed analysis of time-resolved PL spectra (**Figure S1** and **Table S1**) clearly shows that, by means of deconvolution with two Gaussian bands (the fit is carried out in the energy space), a 10% larger contribution of the green band is gathered in the S8-CD hybrid as compared to the S3-CD one. The decay times display a non-single exponential profile due to a fast contribution shorter than 1 ns and a second decay in the 2-3 ns range for the S3-CD and S8-CD samples, with a further longer contribution due to the emission of the silica matrix [78,79] (**Table S2**, the other details are related to photo-physics experiments described in the next section). The overall faster decay time in hybrid samples as compared to CD-R

dispersed in water causes a lower efficiency of the former (QY of about 1%), also due to the large scattering of the excitation by the hybrid powders, being the QY of CD-R of about 5%.

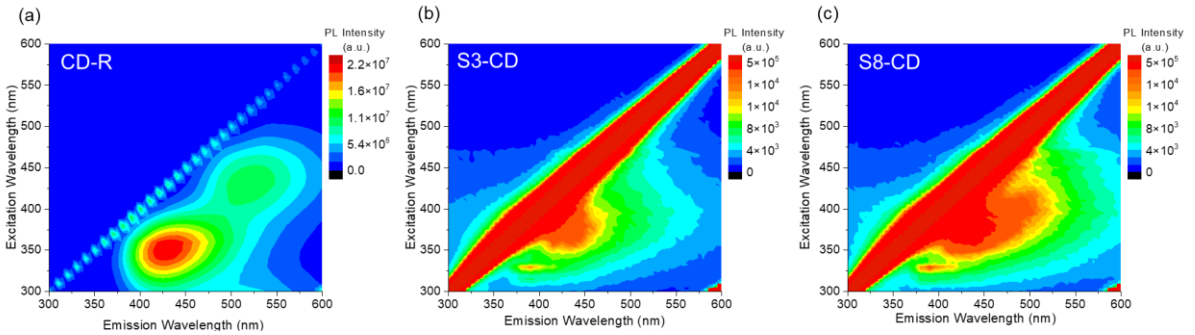

Figure 2. EEMs of CD-R (a), S3-CD (b) and S8-CD (c).

The excitation-emission maps (EEMs) of CD-R dispersed in water and the two S-CD hybrids (**Figure 2**) confirm the scenario reported. Indeed, all the samples present two contributions, as expected from absorption measurements, but while in CDs in water those contributions are well separated and could be assigned to molecular-related centers[20], the emission in the hybrid samples is less defined. A close inspection of the maps reveals that the common blue emission at 430 nm is mainly excited at 350 nm in water whereas in hybrids the excitation peak is shifted to 375 nm. Besides, the green emission is mainly excited at 430 nm and centered at 525 in water whilst it is excited at 400 nm and peaked at 510 nm in hybrids, particularly in the S8-CD sample which shows a larger contribution in this region. It is worth noting that the hybrid green band can be also excited in the near UV region, in opposition to CD-R dispersed in water, whose main green emission is excitable only above 410 nm. These findings suggest that the blue and green emitting centers observed in hybrids samples could be different from the ones displayed in CD-R dispersed in water. These differences can be related to the synthesis conditions (outside and inside silica), the different surrounding environments (water or silica), and the possible concentration effects realized in the hybrid samples. According to the literature [27,80], the observed emission features could be related to intrinsic transitions, usually related to the carbogenic core, or extrinsic transitions due to the presence of dopants, surface centers, or molecular species, the latter being the most efficient ones [31]. The concentration effect is expected to be mainly relevant for the molecular emission centers, whilst less relevant for the core centers and the surface ones. Indeed, no emission could be collected from pure CD-R powders, supporting the hypothesis that concentration phenomena could be responsible for the emission quenching in silica, the interaction with the matrix allowing to observe, on the other hand, the less efficient emission transitions.

In the attempt to associate these optical differences with structural and morphological ones between our CD reference and the hybrid samples, we performed XPS and ATR measurements on CD-R and S-CD powders, along with TEM images of the samples. Once re-scaled for the contribution of silica, XPS measurements report a larger oxygen atomic content in the S3-CD hybrid (38%) at the expense of C and N content (52 and 10%, respectively), whilst the composition of the S8-CD hybrid is much alike the one of the CD reference sample (22, 64 and 14% for O, C and N respectively) with an increase of both absolute and relative to C concentration of N in the latter hybrid (**Table S3**). Whilst the O_{1s} spectrum of both hybrids is due to the large contribution of silica (**Figure S2**, **Table S4**), C_{1s} and N_{1s} spectra allow discussing more in detail the composition in the two sets of samples (**Figure 3**).

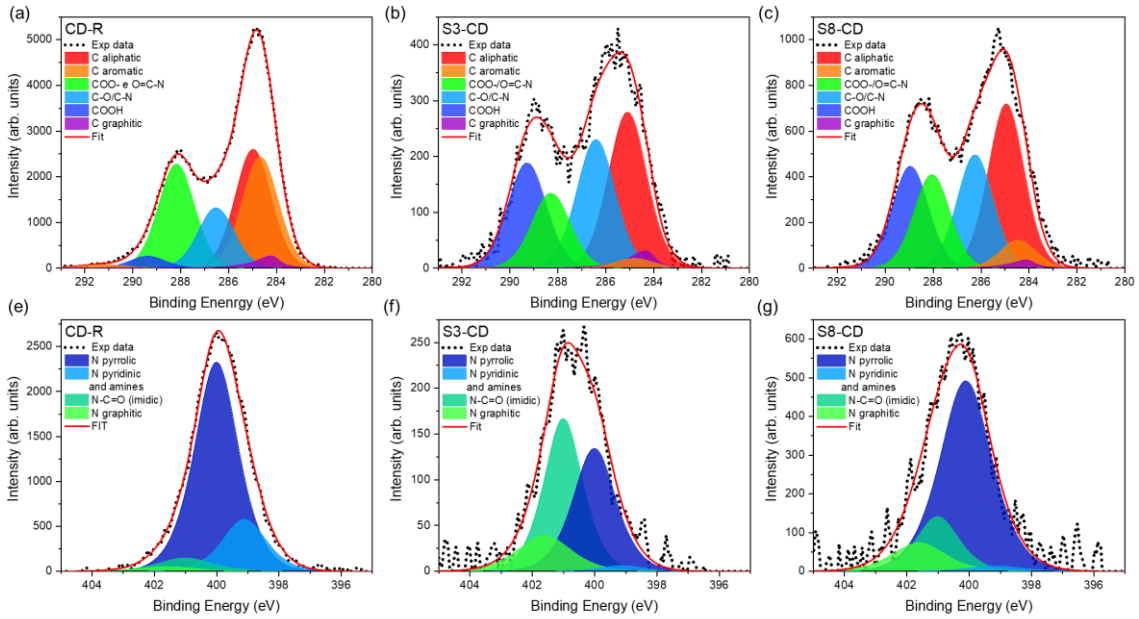

Figure 3. (top) C_{1s} and (down) N_{1s} XPS spectra. On the left of the CD reference sample, in the center of S3-CD, and on the right of S8-CD hybrid samples.

The relative content of organic carbon versus graphitic one is largely affected by the synthesis in the host matrix, being the percentage of graphitic one almost double in S3-CD than in S8-CD hybrid, also higher than in the reference (**Table S5**). These results support the idea that even matrix morphology plays an important role in the structuring of CD nanoparticles. Moreover, in contrast to the reference, silica hybrids have a larger contribution related to the presence of the carboxylic group (about 8 times) and an increase of the signal related to C-O/C-N bonds (about 1.5-2.0 times). The analysis of the N_{1s} spectrum (**Table S6**) clarifies the N contribution, showing a very small content of pyridinic/aminic species in both hybrids as compared to the CD sample (1.8-1.9% against 18.4%) and a larger content of graphitic N (14.4% and 10.8% in S3-CD and S8-CD versus 2% in CD). This is an indication that from one

side no residues from urea pyrolysis are retrieved in the hybrids, from the other side those systems have a larger content of graphitic N and O-related species that calls for different CD structures compared to CD-R, where the contribution of N pyridinic molecules like CZA can be deduced. In addition, the larger content of imidic N gathered in S3-CD (44.4%) and S8-CD hybrid (16.6%) as compared to the reference, and the lower content of pyrrolic N in S3-CD than in S8-CD (39.5 and 70.7% respectively) calls for the presence of imidic HTTP-like centers and could indicate that a complete reaction toward the formation of nitrogen-incorporating emitting centers is not achieved in the former whilst is almost completed in the latter.

The effect of the nanometric size of the porous host exploited as a nano-reactor is also displayed by ATR measurements in the 1900-1500 cm^{-1} range, where the peak of C=O and C=N vibrations are recorded (**Figure S3a**), whilst, excluding this range, the signal of silica matrices hid the expected contribution of other vibrations. The reported spectra display that the relative content of the broad band of the C=C bond in the reference sample (below 1600 cm^{-1}) is largely decreased in the hybrids, where two main contributions are detected at 1650 and 1725 cm^{-1}. The narrow 1725 cm^{-1} band calls for the presence of C=O stretching in aldehydes or esters, with no contribution from ketones or acids, as observed in the reference sample (the broad band with a peak at 1700 cm^{-1}). The large band at 1650 cm^{-1} is ascribed to C=N vibrations, whose relative contribution is larger in S3 hybrids than in S8 ones. These findings agree with the XPS data in suggesting that the silica nanoreactors modify the relative composition and bonding of the synthesized CDs. For the sake of completeness, **Figure S3b** reports the ATR spectrum of CDs dispersed in water showing the fingerprints of the typically observed vibrations (OH, CH, CO, CN, and NH)[65].

As expected from the features of the commercial plain silica samples, TEM images (see **Figure S4**) show the occurrence of mesoporous silicas with monodisperse pore size, with smaller pore size in the S3 sample as compared to S8 sample. From TEM images of the hybrid samples (S3-CD and S8-CD, **Figure S4**) it is not possible to distinctly assess the location of CDs due to the poor contrast ratio. In the attempt to image the CDs and further confirm their presence within silica matrices, we performed a washing procedure of the hybrid samples with water and collected the extracted nanoparticles. The TEM images of these CDs (CD-3 and CD-8) were compared to one of the reference CDs (that is the one synthesized without silica). As reported in **Figure 4** rounded CDs were always observed with a size distribution affected by the interaction with the host matrix. Indeed, whilst reference CDs have a large distribution peaked at about 4.0 nm (SD = 1.1 nm), CD-3 and CD-8 samples have narrower distributions

with mean diameters of 3.2 and 4.4 nm and SD = 0.7 and 0.6 nm respectively. These data confirm that the CD size distribution is affected by the features of the silica support.

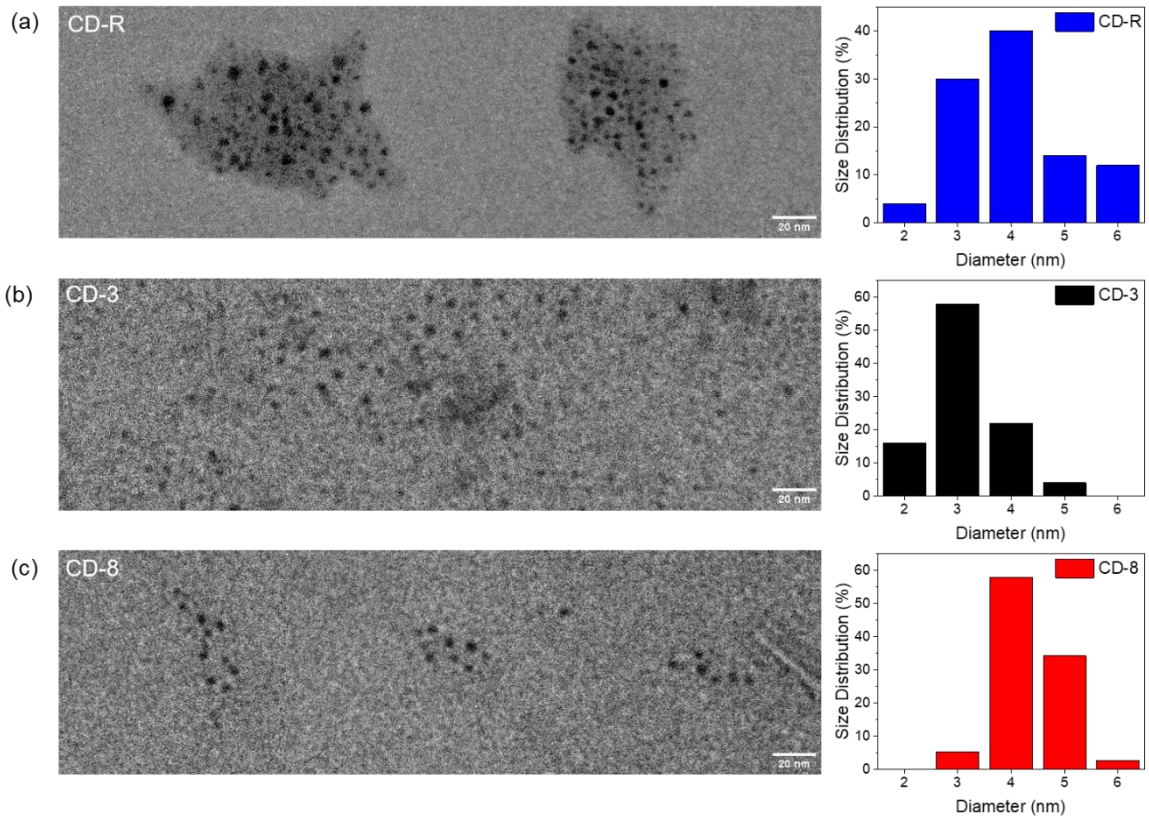

Figure 4. (left) TEM images of CD-R (a), CD-3 (b) and CD-8 (c) with their relative size distribution (right).

A textural investigation was also performed by N_2 physisorption measurements at 77 K, and the obtained isotherms for the S-CD samples (S3-CD and S8-CD) and the corresponding pure SiO_2 (S3, S8) are reported in **Figure S5** and confirm the occurrence of mesoporous silicas with smaller pores in the S3-based samples as compared to S8-based samples. A significant decrease in surface area and pore volume is observed in the hybrid materials as compared to the plain silicas (see **Table S7**). These findings could be due to the occurrence of CDs within the pores of the silica support[81].

Finally, we also carried out the EEM measurements of the extracted CDs dispersed in water (**Figure 5**). The blue and the green emission centers are observed in both samples, with a larger contribution of the green emission with respect to the blue one, as compared to the reference CD samples (**Figure 2a**). The green contribution is even larger in the CD-3 sample than in CD-8 one. The blue emission is peaked at about 450 nm with the main excitation at 365 nm in CD-3, and at 430 nm with excitation at 355 nm in CD-8. As for the green emission, it appears at 525 nm with the main excitation peak at 440 nm in both samples. Interestingly, the QY of these

samples is comparable to the ones of the reference CDs, as reported in **Table S8**. These data clearly show that, even though the hybrid samples have lower efficiency than the reference CD-R samples dispersed in water, the CD-E synthesized in silica display good emission properties once extracted from the host matrices, even restoring their emission efficiency when dispersed in water. Thus, the synthesis in silica allows tuning the size and the optical properties of the prepared CDs.

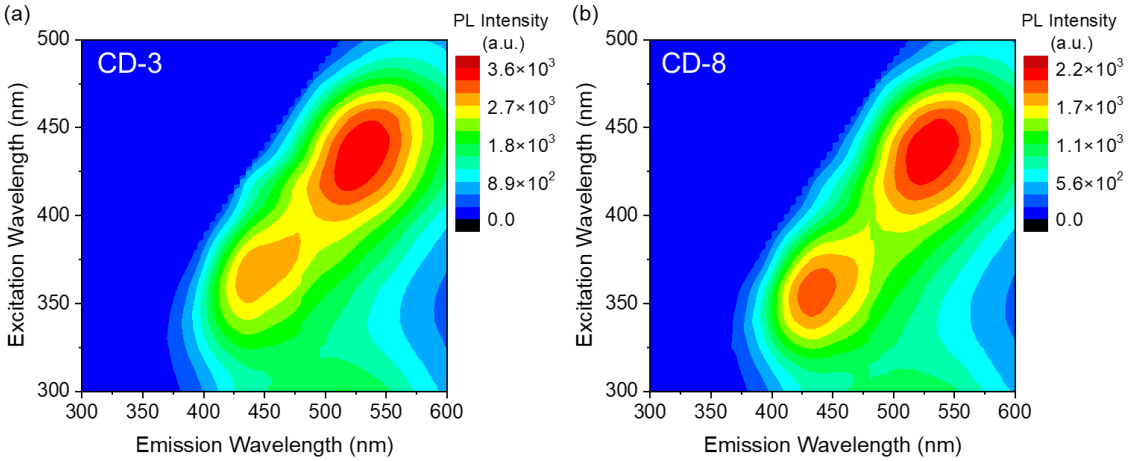

Figure 5. EEM plots of CD-3 (a) and CD-8 (b).

3.2 Photo-physics of CD-silica hybrids

To further discuss the emission features of CD hybrids, we carried out a series of photo-physics experiments by irradiating the samples with femtosecond pulsed and continuous wave (CW) laser light, changing both the excitation power and the irradiation time, and selecting the impinging light within the UV and blue absorption bands of the samples (at 350 nm in the pulsed case, at 405 nm for the CW one). The normalized PL spectra recorded at low and high excitation power (2.5 and 55 μW respectively, **Figure 6**) display that the relative contribution of the green band as compared to the blue one is larger for both the excitation power in S8-CD hybrids than in S3-CD hybrids.

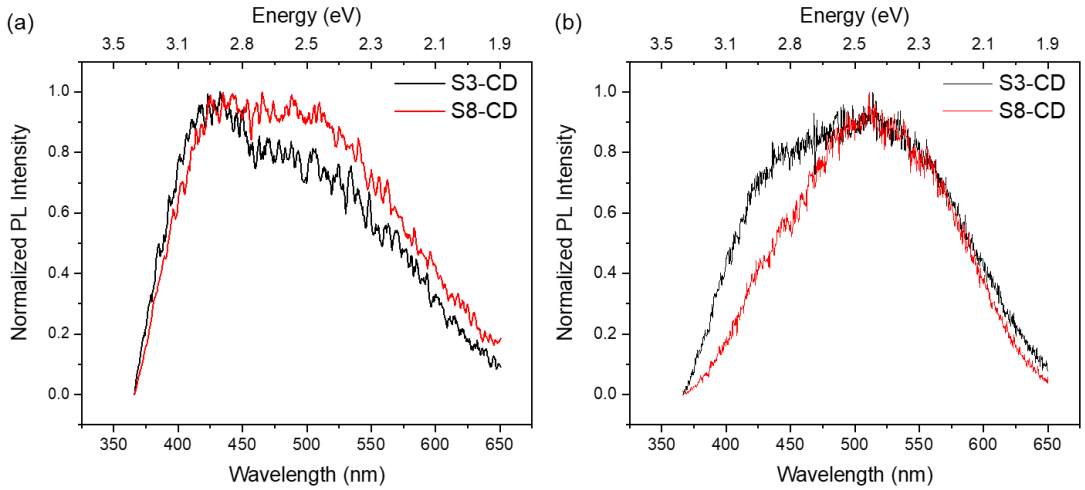

Figure 6. Normalized PL spectra of hybrid samples under 350 nm irradiation at 2.5 μW (a) and 55 μW excitation power (b).

As already anticipated, the fit of the spectra by two Gaussian bands (reported in **Figure S1**) confirms the larger relative content of the green band (74% versus 64% at 2.5 μW and 66% versus 46% W at 55 μW in S8-CD and S3-CD hybrids respectively, see **Table S1**). Those relative contents can be compared to the ones in the CD sample dispersed in water, where they are inverted (73% and 27% for the blue and green emission bands respectively, **Figure S7**). Besides, as already noted before, the spectral features of the two bands excited at 350 nm are also quite different: the blue band is peaked at about 420 and 456 nm in the S-CD hybrids whilst at 440 nm in the CD-R in water, and the green band is centered in the 530-550 nm for the hybrids and at about 510 nm in the reference. The decay time plots (**Figures S1** and **S7)** confirm the interaction of CD with the silica matrix, with a net decrease of the lifetime at both low and high excitation power as compared to CD-R dispersed in water (**Table S2**). The average decay time (see SI for details) was estimated through a non-single exponential decay fit, assuming three decays, with an experimental time resolution of about 0.8 ns over the investigated 100 ns time windows (evaluated using the signal 10%-90% rise time). The decrease in the average decay time from 7 ns to 2-3 ns in hybrid samples is due to the larger relative contribution of the fastest two decays.

The analysis of the spectrum as a function of the excitation power (**Figure 7**) indicates that the relative content of the blue band decreases as the excitation power increases suggesting some photo-activated process involving the blue and green emitting centers.

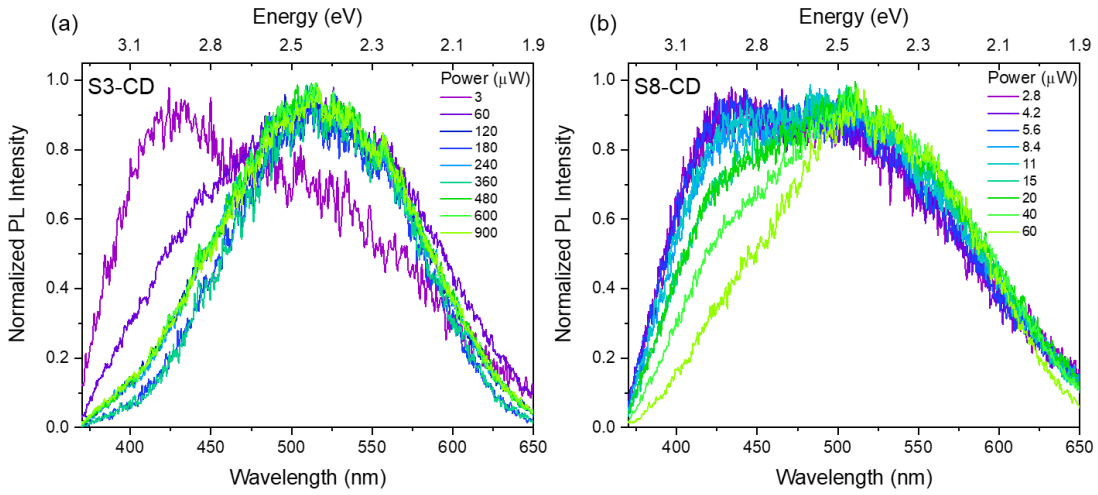

Figure 7. Effect of increasing excitation power on the PL spectra of S8-CD (a) and S3-CD (b) hybrids.

It is interesting to note that the spectral variation is completed in the S8-CD hybrid when the irradiation power achieves 60 μW, whilst it keeps going on in the S3-CD sample up to about 200 μW. At the end of the process both the samples display an emission band peaked at about 520 nm with a reduced relative contribution in the blue range. To clarify the photo-activated process, we performed a photo-kinetic study of the hybrid samples. Indeed, the spectra in **Figure 7** were collected by shining the samples for the time required to achieve a good signal-to-noise ratio, thus representing a sort of averaged effect of excitation power and irradiation time. To follow the variation induced by the irradiation time at a fixed excitation power (2.5, 5, and 55 μW) we performed a series of acquisitions of 5 s over the irradiation time range of 500 s for the lower powers and 0.5 s over 50 s for the highest one. The spectra at the beginning of the experiment and at the end of it are compared in **Figure 8,** showing the same trend reported as a function of the excitation power.

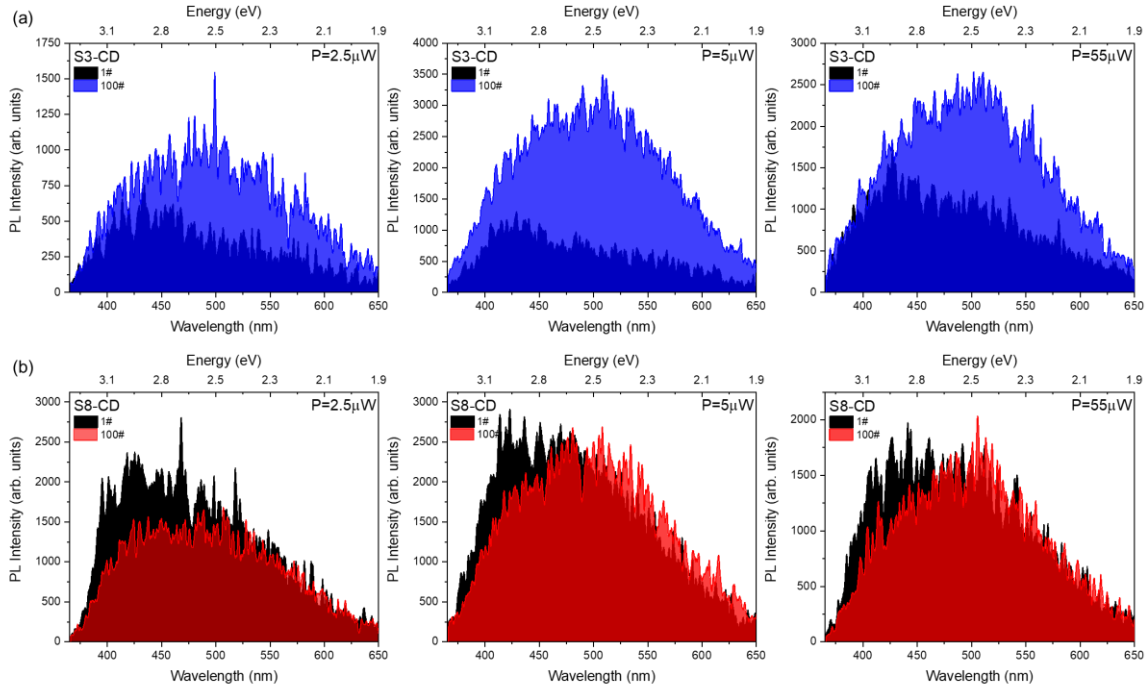

Figure 8. PL spectra of S3-CD (a) and S8-CD (b) hybrids extracted from the irradiation kinetics measurements at 2.5, 5, and 55 μW (round focused spot laser was about 200 μm in diameter).

We see that the observed variation is mainly related to the increase of the green band in S3-CD hybrids whilst in the S8-CD samples the main process is the decrease of the blue band and a slight increase of the green one at the highest excitation power. The full sequence of the kinetics at 5 μW for the two hybrid samples is reported in **Figure 9**.

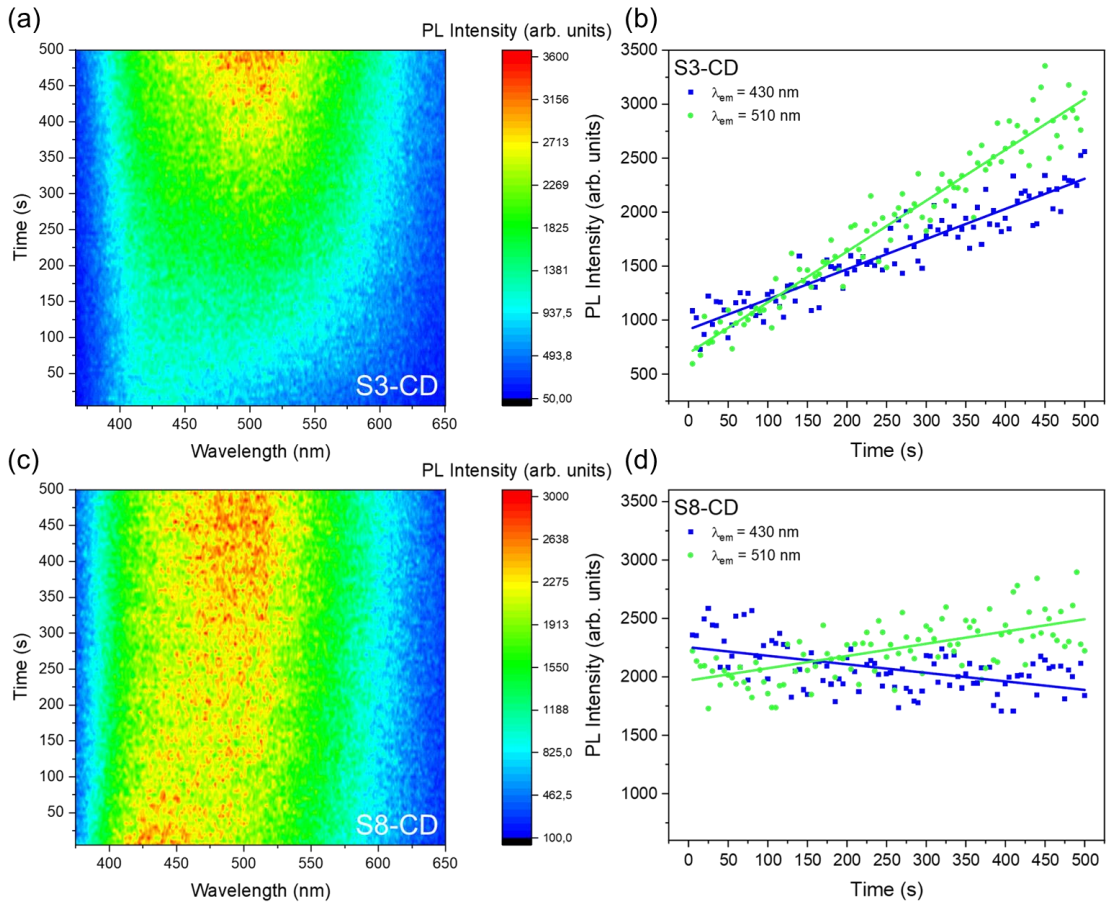

Figure 9. S3 (a) and S8 (c) CD kinetics recorded under 350 nm irradiation at 5 μW. The trend of the PL intensity VS time at selected emission wavelength for S3 (b) and S8 (d) CD samples.

The color maps display that in both cases the overall effect is a greener emission after the whole irradiation sequence coupled with an increase of the blue band in the case of the S3-CD hybrid and a decrease of the same emission in the S8-CD one. The trends are also highlighted by the plot of the PL intensity at 430 and 510 nm in both samples as a function of irradiation time. It is worth noting that all these trends are linear and in the latter case the two trends have equal but opposite slopes. We also observe that the increase rate of the green band in the case of the S3-CD hybrid is five times larger than in the case of the S8-CD one. These findings suggest that in the case of the S3-CD hybrid the irradiation promotes a larger increase of the emitting centers as compared to S8-CD samples, which could be related to the larger content of reaction intermediates observed in the former, as reported by XPS measurements. The effects of CW laser irradiation at 405 nm are also similar, as reported in **Figure S7**, leading to a fast saturation effect on the S8-CD hybrids and a linear increase of the green band in S3-CD samples.

To address the origin of the photo-activated process we performed the photo-physics analysis also on the soaked samples (I-CDs). Indeed, as previously discussed, the CDs synthesized within the silica nanoreactors (S-CDs) have a different composition than the reference CDs (CD-R) synthesized without silica, and different main emitting centers were hypothesized in the two cases, calling for most molecular emitters in the latter and surface centers in the former. Thus, in the case of I-CD samples, we expect that the UV irradiation should affect the emitting molecular centers leading to photobleaching of the samples, as reported in the literature[82].

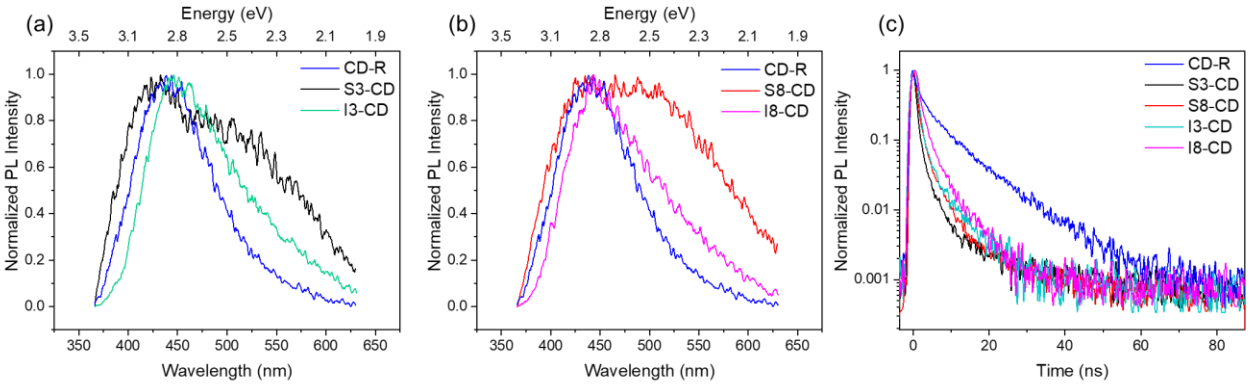

Figure 10. Comparison of PL spectra of reference CD-R dispersed in water, the S-CD hybrids, and the soaked I-CD samples in S3 (MCM-48) (a) and S8 (SBA-15) (b). Decay time plot of the samples excited at 350 nm with 2.5 μW excitation power (c).

As reported in **Figure 10**, the spectral features of the emission in I3-CD and I8-CD hybrids excited at 350 nm are in between the ones of the S-CDs and the CD-R dispersed in water, showing a blue band at about 440 nm and an intermediate relative content of the green band peaked at about 510 nm. The decay time profiles are similar to the ones of S-CD hybrids, calling for the interaction with the porous matrix and concentration-related effects. The recorded kinetic map of I3-CD (**Figure 11**) displayed a large decrease in both the blue and green emissions during the first hundred seconds followed by an increase in the green emission and a constant blue contribution. In the case of I8-CD, we observed only the decrease of the two emission bands with no further modifications. Moreover, the irradiation with CW blue laser of impregnated samples causes the increase of the green band in I3-CD samples and almost no effects on the I8-CD ones (**Figure S7**). The differences recorded in the two silica matrices for both the S-CD and I-CD hybrids could be related to the different content of OH groups in the two matrices, as discussed in the following section (*vide infra*).

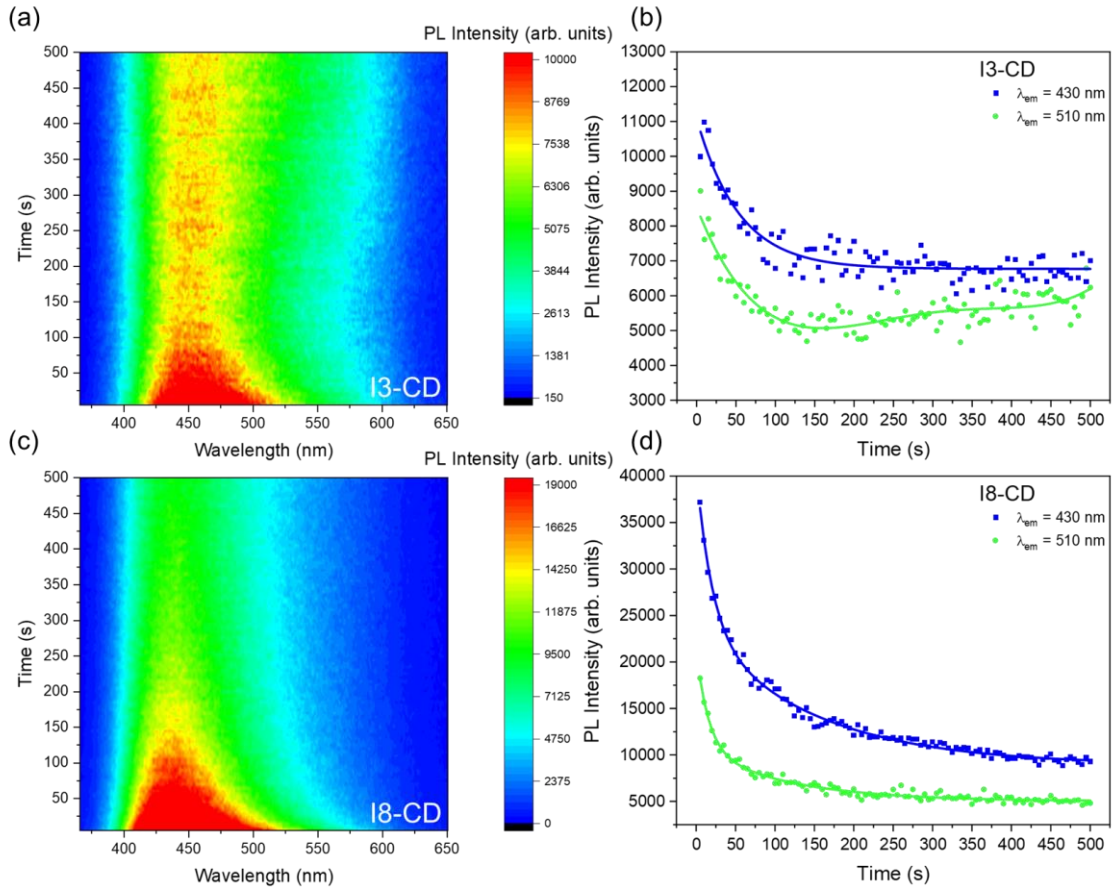

Figure 11. I3 (a) and I8 (c) CD kinetics were recorded under 350 nm irradiation at 5 μW. The trend of the PL intensity VS time at selected emission wavelengths for I3 (b) and I8 (d) CD samples.

To rationalize the data, we pinpoint that no variations were observed in the case of CD-R dispersed in water under different excitations powers of UV irradiation with the same experimental conditions applied for the hybrids (laser beam focused on the front face of the sample, cuvette of 1 cm for the dispersed samples). Indeed, UV photobleaching of CDs dispersed in water was reported when the whole sample was homogenously irradiated [82]. In the present case, the irradiated volume was very small, and the CDs dispersed in water could freely move around the whole cell, thus reducing the probability of being photobleached or modified by UV irradiation. The reported photo-physics effects are peculiar to the hybrid systems and the interaction of CDs with the silica host matrix. Indeed, not only did we observe a starting emission with a larger contribution in the green range as compared to the CDs in water in both the matrices, but also a larger surface photo-reactivity that further promoted the formation of green-emitting centers, eventually to the expense of the blue ones. The photo-activated process is mediated by the presence of the silica matrix, thus ascribing the recorded

emission features to surface centers interacting with the surrounding environment. The results gathered with impregnated hybrid samples further support this hypothesis, showing first a decrease in the molecular emission features and then an increase in the contribution of surface states, in agreement with previous results on CDs dispersed in water[83].

A few conclusions can be drawn from the overall reported experimental data, further considered to guide the computational work: the interaction of silica host with CDs produces a broader emission spectrum than for CDs dispersed in water, with a larger relative contribution of the green emission as compared to the blue one. The interaction with the matrix is demonstrated by the decrease of the average decay time of the emission because of non-radiative transitions mediated by the host also decreasing the overall emission efficiency. Aggregation phenomena of CDs within the silica may also decrease the global QY, in particular with reference to the molecular states. The emitting centers have different spectral features for hybrids and dispersed CDs, calling mostly for surface emitting centers in the first case and molecular centers in the second one. The structural analysis confirms this hypothesis since CDs in hybrid systems have a larger relative content of O and N as compared to CD sample in water. The larger content of O produces an increase in the OH and COOH groups, whilst the N relative increase is mainly related to a larger content of graphitic N. The comparison of the kinetics recorded under prolonged laser irradiation of S-CD and I-CD hybrids further confirms the proposed interpretation, showing that the photo-activated interaction with the silica matrix modifies the relative content of emitting surface centers in S-CD hybrids, leading to the increase of the emission in the green spectral range. In I-CD hybrids we mainly observe the photobleaching of the emitting molecular species, and eventually the increase of the surface ones.

3.3 DFT and TD-DFT calculations

To understand the interactions of CDs embedded in the hybrid systems, selected models of carbon dots within the silica host pores were studied by DFT and TD-DFT calculations. We considered a 14 Si atoms model of silica, already reported for simulating defects in silica[65,72], and a set of possible CD-related systems, including OH and COOH edge functional groups on a pyrene model structure (PYR-OH, PYR-COOH, and PYR respectively), a graphitic N inside the pyrene model structure (PYR-NGRAPH) and two selected molecules, CZA and the HPPT, which could be formed during the citric acid synthesis and represent the prototype of pyridinic and imidic molecular centers (**Figure 10**). It is known, indeed, that OH and COOH functional groups allow red shifting of the optical properties of CDs [27,84], thus

potentially contributing to the emission in the blue-green spectral range. In addition, the insertion of N in the PAH network in the form of graphitic N produces a large redshift of the pristine PAH model[4,85], giving rise to emission in the green spectral range. For these reasons, and accounting for the experimental findings, we considered the pyrene structure as a reference PAH model and modified the system by adding an OH or COOH functional group on the edge of the pristine pyrene structure. Similarly, we inserted a graphitic N in the structure to test the formation of CDs with larger content of N within the C network. Besides, as discussed in the introduction, we considered CZA and HPPT molecules whose formation could be expected in the present synthesis, as suggested by the recorded absorption and emission features (**Figure 1** and **Figure 2**). Concerning the silica models here considered, with full H, full OH, and partial OH (1 and 4 OH) termination, the four models produced similar UV optical absorption peaked around 170 nm (**Figure S8**). It is worth underlining that we do not consider any solvent effect in the reported calculations, since the synthesis was performed under solvent-free conditions.

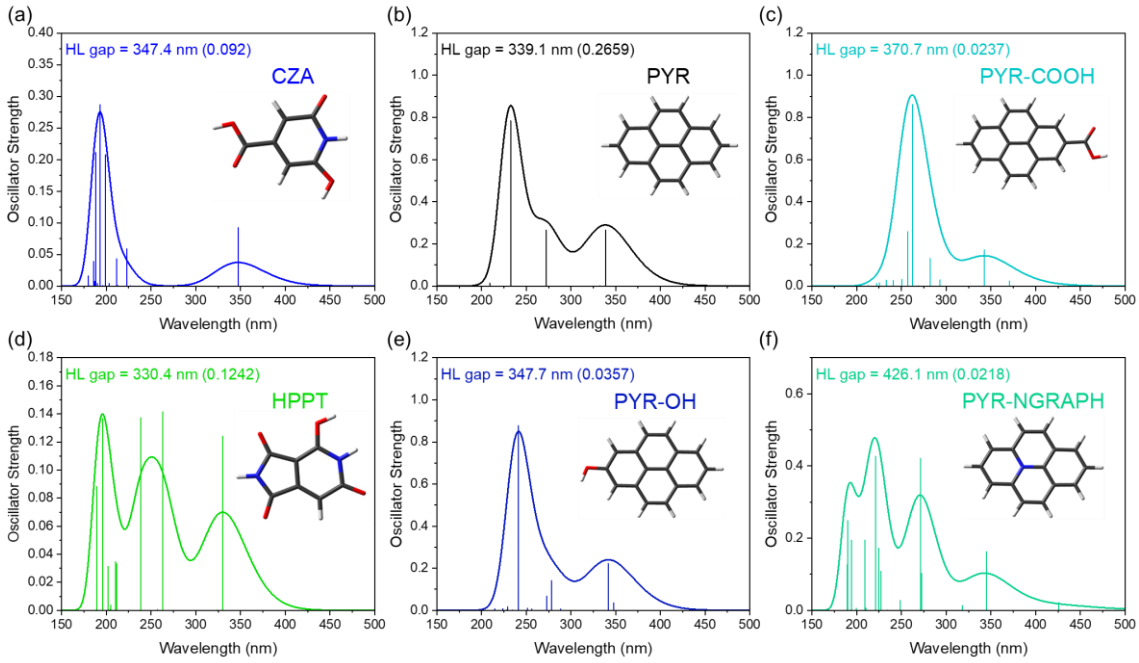

Figure 12: Calculated optical absorption features of isolated emitting center models (simplified stick representation: white stick = H atom, dark grey stick = C atom, red stick = O atom, and blue stick = N atom).

As reported in **Figure 12**, the presence of OH and COOH functional groups at the edge of our pyrene reference model produces a red shift of the HOMO-LUMO (HL) gap, from 339 nm to 347 and 370 nm for the OH and COOH group respectively, also largely reducing the oscillator strength of the transition in both cases. These findings are in good agreement with previous results and suggest that these surface emitting centers could be responsible for a blue

emission (OH) and a cyan emission (COOH) respectively, whilst the carbogenic core could be responsible for near UV-blue contributions[8]. The model with graphitic N shows a larger redshift of the HL gap, moving the transition up to 426 nm, thus fully supporting the possible attribution of the green emission to the presence of graphitic N[27]. However, the oscillator strength is reduced also in this case by about one order of magnitude as compared to the pristine undoped model. Concerning the two molecules, the results on CZA agree with previously reported ones[40,74], calling for the assignment of the blue emission to this molecule when a blue molecular center is observed. Surprisingly, the results on HPPT do show an absorption transition at 330 nm, quite far away from the expected absorption at about 400 nm experimentally reported[20] and recently calculated but to a lower theory level (B3LYP and 6-31G(d,p) basis set[86]) for the anionic form of HPPT. A theoretical in-depth analysis of these results is beyond the scope of the present research and will be discussed in further work. Interestingly, both molecular species, CZA and HPPT, have larger oscillator strength than the other models here considered, thus providing more efficient emissions in the blue (CZA) and the green (HPPT) spectral range.

To mimic the interaction with the silica surface, we hypothesized a simplified model where the emitting centers are placed at the surface of the CD, either that they were molecules, like CZA and HPPT, or surface functional groups, like OH and COOH, or graphitic N within pyrene structures. The model centers can face the silica surface in a parallel or orthogonal way, assuming the centers are positioned at the CD surface as orthogonal spikes or as surface planar structures, as previously proposed[25,26]. This is clearly a simplified scheme since all the possible interaction angles between the silica surface and the centers should be considered. In addition, there are also many possible sites at the silica surface where our models can express their interaction with the matrix, thus making the configurational space of the interacting systems very large. Besides, we are not considering, as stated before, any possible homo or hetero aggregation between emitting species, which could be even favored by the CD-supporting surface[65,66,87]. Starting from the simplified assumptions made, Potential Energy Surfaces (PESs) were calculated to explore the interaction between CDs and silica along selected trajectories to specific interaction silica sites and performing rigid scan calculations, not allowing the silica network nor the emitting species to modify their structure during the scan. Finally, no PES were calculated for the pyrene system, since the carbogenic core is expected to be not affected by the interaction with the surrounding media.

As illustrated in **Figure 13** for the representative case of CZA, an energy minimum was obtained for the whole set of selected trajectories for the orthogonal relative position of the

considered emitting center model with respect to the silica surface. In the case of CZA and HPPT also parallel orientation gave a minimum in the computed PES. We also calculated the relaxed geometries starting from the minima of the rigid scan PES calculations and letting the full system relax. The whole set of model systems did relax in a normal or slightly oblique position with respect to the silica surface, also the CZA and HPPT molecules when starting from the parallel one. Thus, for the configurations in the total energy minima of fixed and relaxed geometries, we calculated the absorption spectrum of the system, and the oscillator strength of the HL gap and compared the data to the results for the isolated model structures. The optical features recorded for the fixed and relaxed configurations were very similar for both the HL gap position and its oscillator strength.

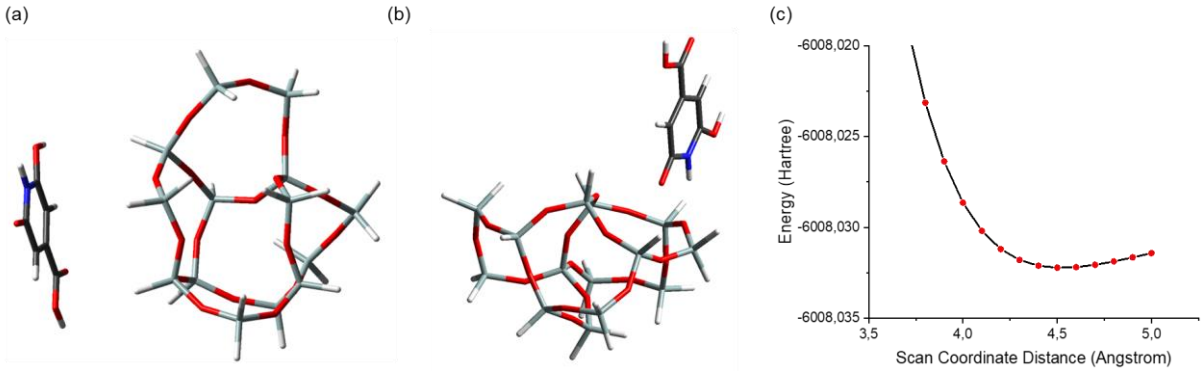

Figure 13. Schematic representation of CZA-silica relative position and PES trajectory for the parallel (a) and orthogonal (b) case. The calculated PES for the orthogonal case is reported in (c). Simplified stick representation: white stick = H atom, dark grey stick = C atom, light grey stick = Si atom, red stick = O atom, and blue stick = N atom.

The comparison of the HL gap of isolated and interacting with silica model structures, considering both fully H and OH terminated silica, shows interesting results (**Figure 14**): in general, the gap position is slightly affected by the interaction with the silica matrix but for the HPPT case, where a large redshift up to about 400 nm is recorded. Besides red shifting, the oscillator strength of HPPT interacting with silica (fully H terminated model) is slightly increased (+1.4%), like the one of graphitic N system (+1.4%). The COOH model also experiences an increase in the transition efficiency, of about +8.4%, whilst the OH model system and CZA undergo a decrease in their oscillator strength (-25.3% and -4.5% respectively). Thus, the overall effect is an increase in the efficiency of the cyan and green emitting centers as compared to the blue ones, for both surface state and molecular state models, in very good agreement with the experimental findings. Similar results also hold for the fully OH terminated silica but for a large increase of the oscillator strength of the OH model system

(+59.9%) and a decrease of the COOH system one (-8.9%) suggesting that the presence of water at the silica surface would blue shift the overall emission of CDs, as for the CDs dispersed in water.

Finally, we considered the possible presence of a few OH groups at the silica surface (1 and 4) and calculated the optical features of the system when the molecules interact with the silica surface in the nearby hydroxyl groups. The HL gap did not change so much for the OH, COOH, and graphitic N model systems, whilst a larger blue shift as compared to the full H or OH silica coverage was recorded for the CZA and HPPT molecules (**Figure S9**). Besides, the oscillator strength changed a lot, in particular for the PYR-OH model system, suggesting that the interaction largely depends on the selected sites and on the eventual presence of OH groups which could promote, once again, the blue emission.

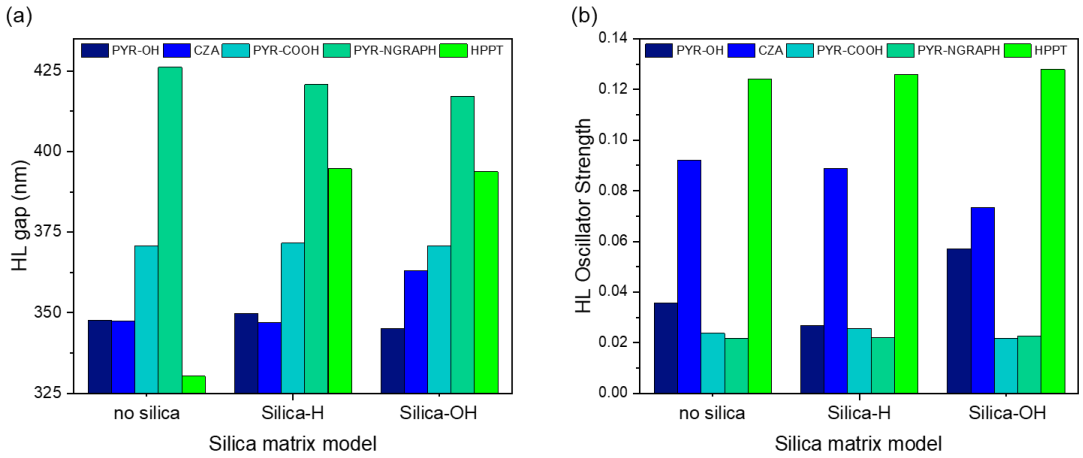

Figure 14: HL gap (left) and oscillator strength (right) for the different model structures without silica, or in presence of fully H-terminated or fully OH-terminated silica models.

To sum up all the simulations, the formation of graphitic N systems or HPPT molecules (here considered as a prototype of imidic molecular centers) can explain the observed green emission for the silica-CD hybrids, the interaction with the silica surface promoting the redshift of the HPPT HL gap, and the increase of the oscillator strength of both models. The other models here considered, OH and COOH pyrene structures and CZA molecule, have optical features that could explain the observed blue emission (OH system and CZA) or cyan emission (COOH system) contributing to the overall emission spectrum of the hybrid systems with lower efficiency than in outside silica CDs. Despite the necessary simplifications in the studied models compared to the experimental samples, the reported computational results do explain the experimental data of CD samples in silica, where the interaction with the host matrix promotes the emission in the green range with respect to the blue one, in particular for the S8

silica. However, the presence of OH groups on the silica surface can largely affect the relative content of blue and green emissions, as gathered from the simulated interactions with silica fully or partially covered with OH groups. Indeed, the models associated with the blue emission displayed, on average, larger oscillator strength when OH groups are at the silica surface, also depending on the selected interaction site. The larger values of oscillator strength calculated for those model systems can explain the differences recorded between the two hybrid structures since a larger content of OH groups could be expected in the mesoporous matrix with lower pore volume (0.5 cm^3/g and 1.0 cm^3/g in S3 and S8 respectively) and larger specific surface area (1500 m^2/g and 500 m^2/g for S3 and S8 respectively)[88]. These differences could explain from one side the different atomic content and chemical bonding observed in the two hybrids, on the other side could be also relevant for the photo-induced effects observed in the photo-physic experiments. Indeed, the hybrid samples were prepared with a solvent-free synthesis, and we should expect that no water could remain within the pores. However, some OH groups could cover the inner surface of the pores (with a larger concentration in smaller pore matrices, as explained above), thus influencing the interaction of CDs with the silica surface. According to the results of the simulations, on average, the presence of OH groups on the silica surface favors the blue-emitting model systems. Upon laser irradiation those OH groups on the silica surface could be removed, thus reducing the blue emission contributions, and promoting the luminescence of the green emitting model systems, the effect being more important in the silica matrices with larger content of OH groups at the surface.

A final comment regards the contribution of molecular and surface centers. The molecular contribution is largely quenched in silica hybrids because of aggregation phenomena. Indeed, once the CDs are extracted from the host matrices (CD-E) and dispersed in water their QY is restored, and a large green emission probably due to some imidic molecular center is observed. However, we have shown that the computed interaction with the silica matrix promotes the green emitting centers when the content of hydroxyl groups on the silica surface is reduced and the blue emitting ones when the latter is increased. This observation holds for both the molecular and surface-emitting centers suggesting that if one could reduce the aggregation phenomena within the porous host, also the molecular centers could provide their contribution to the overall emission[89]. As a consequence, an increase in the QY of the hybrid systems could be expected because of their larger oscillator strength as compared to the surface centers. This indication agrees with the results reported to mitigate the concentration phenomena for dyes in solid-state applications[90] prompting the research on solid CDs towards an efficient

mechanism of nanoparticle separation able to preserve the beneficial interaction with the supporting media.

4. Conclusions

The production of CDs-silica hybrids in silica matrices with different pore sizes and textures allowed discussing the formation of blue and green emitting CDs, by means of a multi-technique approach combined with quantum chemistry computations. We first assessed the possibility of producing the nanoparticles with a solvent-free synthesis, with spectral features in agreement with the ones of other solvent-mediated methods. As compared to nanoparticles dispersed in water, the hybrids show a larger relative content of the green emission which undergoes an increase under UV or blue irradiation, in particular for the matrix with smaller pores and larger interconnection. Higher content of graphitic N, O-related species, and imidic groups and a lower content of pyridinic one was measured in both hybrids as compared to reference CDs, suggesting that the nano-reactors favor the inclusion of N atoms within the C network of the nanoparticles and change the relative content of molecular centers. The reported analysis calls for a different distribution of emitting states in the hybrid samples as compared to the CDs dispersed in water, also related to the environment surrounding the nanoparticles: in the first ones we mostly observe the emission from surface centers, and in the second ones mostly from molecular centers. Indeed, the concentration effect of nanoparticles within the host matrix further reduces the contribution from molecular centers in the hybrid samples. This hypothesis is confirmed by the investigation of the hybrids prepared by imbibition of reference CDs into the silica matrices, the photo-physics experiments displaying a large decrease of the overall molecular emission followed by the increase of the surface center contribution. The larger efficiency of the green emitting centers in silica as compared to the blue emitting ones was explained by performing quantum chemistry calculations on the interaction between silica surface and possible models of fluorescent centers, like OH and COOH surface groups, graphitic N, and citric acid-based prototype molecules, namely CZA and HPPT. The analysis of the computed optical features of the interacting systems confirmed that the host-guest interaction can affect both the spectral features and the efficiency of their transition. Indeed, the HL gap of HPPT is red-shifted because of the interaction with the silica surface, and the oscillator strength of the cyan (COOH) and green emitting centers (graphitic N and HPPT) is increased, whilst the efficiency of the transitions of the blue emitting centers (OH and CZA) is decreased. Thus, the overall effect is promoting green emission, as experimentally observed. Computational results also indicate that the presence of OH groups on the silica surface can

modify this overall effect, boosting the efficiency of blue emitting centers and further confirming the active role of the silica surface in tuning the optical properties of embedded CDs. Finally, the CD extracted from the silica matrices and dispersed in water restored their quantum yield and displayed a larger molecular-like green contribution. The simulations also indicate that if proper strategies to overcome aggregation phenomena are applied, the interaction with the silica matrix would be advantageous also for the more efficient molecular centers. Despite the low efficiency of the synthesized hybrid systems, mainly due to aggregation phenomena, we have shown that the mesoporous silicas are useful as nanoreactors and active support to host CD nanoparticles, exploitable as a lever for tuning the size and optical properties of CDs for both in solution and solid-state applications.

Supporting Information

Supporting Information is available from the publisher or from the author.

Acknowledgements

We acknowledge the CeSAR (Centro Servizi d'Ateneo per la Ricerca) of the University of Cagliari, Italy for ultrafast optical spectroscopy measurements and TEM imaging. Franca Sini is acknowledged for physisorption measurements. Italian Ministry of University and Research (MIUR) within the project PRIN2017 “CANDL2” (Grant 2017W75RAE) and “Fondazione di Sardegna” within the project L.R 7. CUP F74I19000930007 “NG-Light: a new generation of phosphors” are gratefully acknowledged.

Conflict of Interest

The authors declare no conflict of interest.

Abbreviations

CD, carbon dot, CZA, citrazinic acid, HPPT, 4-hydroxy-1H-pyrrolo[3,4-c]pyridine-1,3,6(2H,5H)-trione, TEM, transmission electron microscopy, XPS, X-ray photoelectron spectroscopy, FTIR, Fourier-transform infrared spectroscopy, PL, photoluminescence, TR-PL, time resolved PL, DFT, density functional theory, TD-DFT, time-dependent DFT, PES, potential energy surface.

References

[1] F. Yan, Z. Sun, H. Zhang, X. Sun, Y. Jiang, Z. Bai, The fluorescence mechanism of carbon dots, and methods for tuning their emission color: a review, Microchimica Acta. 186 (2019). https://doi.org/10.1007/s00604-019-3688-y.

[2] W.U. Khan, D. Wang, W. Zhang, Z. Tang, X. Ma, X. Ding, S. Du, Y. Wang, High quantum yield green-emitting carbon dots for Fe(III) detection, biocompatible fluorescent ink and cellular imaging, Sci Rep. 7 (2017) 1–9. https://doi.org/10.1038/s41598-017-15054-9.

[3] H. Liu, Z. Li, Y. Sun, X. Geng, Y. Hu, H. Meng, J. Ge, L. Qu, Synthesis of Luminescent Carbon Dots with Ultrahigh Quantum Yield and Inherent Folate Receptor-Positive Cancer Cell Targetability, Sci Rep. 8 (2018) 1–8. https://doi.org/10.1038/s41598-018-19373-3.

[4] K. Holá, M. Sudolská, S. Kalytchuk, D. Nachtigallová, A.L. Rogach, M. Otyepka, R. Zbořil, Graphitic Nitrogen Triggers Red Fluorescence in Carbon Dots, ACS Nano. 11 (2017) 12402–12410. https://doi.org/10.1021/ACSNANO.7B06399.

[5] M. Sudolská, M. Otyepka, Exact roles of individual chemical forms of nitrogen in the photoluminescent properties of nitrogen-doped carbon dots, Appl Mater Today. 7 (2017) 190–200. https://doi.org/10.1016/J.APMT.2017.03.004.

[6] E. V. Kundelev, N. V. Tepliakov, M.Y. Leonov, V.G. Maslov, A. V. Baranov, A. V. Fedorov, I.D. Rukhlenko, A.L. Rogach, Amino Functionalization of Carbon Dots Leads to Red Emission Enhancement, Journal of Physical Chemistry Letters. 10 (2019) 5111–5116. https://doi.org/10.1021/acs.jpclett.9b01724.

[7] Y. Xie, X. Geng, J. Gao, W. Shi, Z. Zhou, H. Wang, D. Zhang, B. Deng, R. Yu, Synthesis of carbon dots@Mg(OH)2 solid-state composites with blue, red emitting for horticultural application, J Alloys Compd. 873 (2021) 159663. https://doi.org/10.1016/J.JALLCOM.2021.159663.

[8] C.M. Carbonaro, D. Chiriu, L. Stagi, M.F. Casula, S. v. Thakkar, L. Malfatti, K. Suzuki, P.C. Ricci, R. Corpino, Carbon Dots in Water and Mesoporous Matrix: Chasing the Origin of their Photoluminescence, Journal of Physical Chemistry C. 122 (2018) 25638–25650. https://doi.org/10.1021/acs.jpcc.8b08012.

[9] D. Xu, Q. Lin, H.T. Chang, Recent Advances and Sensing Applications of Carbon Dots, Small Methods. 4 (2020). https://doi.org/10.1002/smtd.201900387.

[10] P. He, Y. Shi, T. Meng, T. Yuan, Y. Li, X. Li, Y. Zhang, L. Fan, S. Yang, Recent advances in white light-emitting diodes of carbon quantum dots, 12 (2020) 4826. https://doi.org/10.1039/c9nr10958g.

[11] D. Qu, X. Wang, Y. Bao, Z. Sun, Recent advance of carbon dots in bio-related applications, JPhys Materials. 3 (2020). https://doi.org/10.1088/2515-7639/ab7cb9.

[12] S. Kalytchuk, L. Zdražil, Z. Bad'ura, M. Medved', M. Langer, M. Paloncýová, G. Zoppellaro, S. V. Kershaw, A.L. Rogach, M. Otyepka, R. Zbořil, Carbon Dots Detect Water-to-Ice Phase Transition and Act as Alcohol Sensors via Fluorescence Turn-Off/On Mechanism, ACS Nano. 15 (2021) 6582–6593. https://doi.org/10.1021/ACSNANO.0C09781.

[13] L. Wang, H. Zhang, X. Zhou, Y. Liu, B. Lei, Preparation, characterization and oxygen sensing properties of luminescent carbon dots assembled mesoporous silica microspheres, J Colloid Interface Sci. 478 (2016) 256–262. https://doi.org/10.1016/j.jcis.2016.06.026.

[14] Z. Wang, C. Xu, Y. Lu, F. Wu, G. Ye, G. Wei, T. Sun, J. Chen, Visualization of Adsorption: Luminescent Mesoporous Silica-Carbon Dots Composite for Rapid and Selective Removal of U(VI) and in Situ Monitoring the Adsorption Behavior, ACS Appl Mater Interfaces. 9 (2017) 7392–7398. https://doi.org/10.1021/acsami.6b13427.

[15] M. Liu, T. Li, C. Zhang, Y. Zheng, C. Wu, J. Zhang, K. Zhang, Z. Zhang, Fluorescent carbon dots embedded in mesoporous silica nanospheres: A simple platform for Cr(VI) detection in environmental water, J Hazard Mater. 415 (2021) 125699. https://doi.org/10.1016/j.jhazmat.2021.125699.
[16] K.J. Mintz, Y. Zhou, R.M. Leblanc, Recent development of carbon quantum dots regarding their optical properties, photoluminescence mechanism, and core structure, Nanoscale. 11 (2019) 4634–4652. https://doi.org/10.1039/c8nr10059d.
[17] M. Shamsipur, A. Barati, A.A. Taherpour, M. Jamshidi, Resolving the Multiple Emission Centers in Carbon Dots: From Fluorophore Molecular States to Aromatic Domain States and Carbon-Core States, Journal of Physical Chemistry Letters. 9 (2018) 4189–4198. https://doi.org/10.1021/acs.jpclett.8b02043.
[18] L. Ai, Y. Yang, B. Wang, J. Chang, Z. Tang, B. Yang, S. Lu, Insights into photoluminescence mechanisms of carbon dots: advances and perspectives, Sci Bull (Beijing). 66 (2021) 839–856. https://doi.org/10.1016/j.scib.2020.12.015.
[19] Y. Xiong, J. Schneider, C.J. Reckmeier, H. Huang, P. Kasák, A.L. Rogach, Carbonization conditions influence the emission characteristics and the stability against photobleaching of nitrogen doped carbon dots, Nanoscale. 9 (2017) 11730–11738. https://doi.org/10.1039/c7nr03648e.
[20] W. Kasprzyk, T. Świergosz, S. Bednarz, K. Walas, N. V. Bashmakova, D. Bogdał, Luminescence phenomena of carbon dots derived from citric acid and urea – a molecular insight, Nanoscale. 10 (2018) 13889–13894. https://doi.org/10.1039/C8NR03602K.
[21] F. Ehrat, S. Bhattacharyya, J. Schneider, A. Löf, R. Wyrwich, A.L. Rogach, J.K. Stolarczyk, A.S. Urban, J. Feldmann, Tracking the Source of Carbon Dot Photoluminescence: Aromatic Domains versus Molecular Fluorophores, Nano Lett. 17 (2017) 7710–7716. https://doi.org/10.1021/ACS.NANOLETT.7B03863.
[22] Y. Xiong, J. Schneider, E. V. Ushakova, A.L. Rogach, Influence of molecular fluorophores on the research field of chemically synthesized carbon dots, Nano Today. 23 (2018) 124–139. https://doi.org/10.1016/j.nantod.2018.10.010.
[23] M. Langer, T. Hrivnák, M. Medved', M. Otyepka, Contribution of the Molecular Fluorophore IPCA to Excitation-Independent Photoluminescence of Carbon Dots, The Journal of Physical Chemistry C. 125 (2021) 12140–12148. https://doi.org/10.1021/acs.jpcc.1c02243.
[24] Y. Song, S. Zhu, S. Zhang, Y. Fu, L. Wang, X. Zhao, B. Yang, Investigation from chemical structure to photoluminescent mechanism: a type of carbon dots from the pyrolysis of citric acid and an amine, J Mater Chem C Mater. 3 (2015) 5976–5984. https://doi.org/10.1039/C5TC00813A.
[25] N. V. Tepliakov, E. V. Kundelev, P.D. Khavlyuk, Y. Xiong, M.Y. Leonov, W. Zhu, A. V. Baranov, A. V. Fedorov, A.L. Rogach, I.D. Rukhlenko, sp2-sp3-Hybridized Atomic Domains Determine Optical Features of Carbon Dots, ACS Nano. 13 (2019) 10737–10744. https://doi.org/10.1021/acsnano.9b05444.
[26] E. V. Kundelev, N. V. Tepliakov, M.Y. Leonov, V.G. Maslov, A. V. Baranov, A. V. Fedorov, I.D. Rukhlenko, A.L. Rogach, Toward Bright Red-Emissive Carbon Dots through Controlling Interaction among Surface Emission Centers, Journal of Physical Chemistry Letters. 11 (2020) 8121–8127. https://doi.org/10.1021/acs.jpclett.0c02373.
[27] F. Mocci, L. de Villiers Engelbrecht, C. Olla, A. Cappai, M.F. Casula, C. Melis, L. Stagi, A. Laaksonen, C.M. Carbonaro, Carbon Nanodots from an In Silico Perspective, Chem Rev. 122 (2022) 13709–13799. https://doi.org/10.1021/acs.chemrev.1c00864.
[28] R. Ludmerczki, S. Mura, C.M. Carbonaro, I.M. Mandity, M. Carraro, N. Senes, S. Garroni, G. Granozzi, L. Calvillo, S. Marras, L. Malfatti, P. Innocenzi, Carbon Dots from Citric Acid and its Intermediates Formed by Thermal Decomposition, Chemistry -

A European Journal. 25 (2019) 11963–11974. https://doi.org/10.1002/chem.201902497.
[29] Z. Qian, J. Ma, X. Shan, H. Feng, L. Shao, J. Chen, Highly luminescent N-doped carbon quantum dots as an effective multifunctional fluorescence sensing platform, Chemistry - A European Journal. 20 (2014) 2254–2263. https://doi.org/10.1002/chem.201304374.
[30] J. Liao, Z. Cheng, L. Zhou, Nitrogen-Doping Enhanced Fluorescent Carbon Dots: Green Synthesis and Their Applications for Bioimaging and Label-Free Detection of Au3+ Ions, ACS Sustain Chem Eng. 4 (2016) 3053–3061. https://doi.org/10.1021/acssuschemeng.6b00018.
[31] S. Mura, R. Ludmerczki, L. Stagi, S. Garroni, C.M. Carbonaro, P.C. Ricci, M.F. Casula, L. Malfatti, P. Innocenzi, Integrating sol-gel and carbon dots chemistry for the fabrication of fluorescent hybrid organic-inorganic films, Sci Rep. 10 (2020) 4770. https://doi.org/10.1038/s41598-020-61517-x.
[32] J. Schneider, C.J. Reckmeier, Y. Xiong, M. von Seckendorff, A.S. Susha, P. Kasák, A.L. Rogach, Molecular Fluorescence in Citric Acid-Based Carbon Dots, Journal of Physical Chemistry C. 121 (2017) 2014–2022. https://doi.org/10.1021/ACS.JPCC.6B12519.
[33] F. Meierhofer, F. Dissinger, F. Weigert, J. Jungclaus, K. Müller-Caspary, S.R. Waldvogel, U. Resch-Genger, T. Voss, Citric Acid Based Carbon Dots with Amine Type Stabilizers: PH-Specific Luminescence and Quantum Yield Characteristics, Journal of Physical Chemistry C. 124 (2020) 8894–8904. https://doi.org/10.1021/acs.jpcc.9b11732.
[34] W. Wang, B. Wang, H. Embrechts, C. Damm, A. Cadranel, V. Strauss, M. Distaso, V. Hinterberger, D.M. Guldi, W. Peukert, Shedding light on the effective fluorophore structure of high fluorescence quantum yield carbon nanodots, RSC Adv. 7 (2017) 24771–24780. https://doi.org/10.1039/C7RA04421F.
[35] S. Mura, L. Stagi, L. Malfatti, C.M. Carbonaro, R. Ludmerczki, P. Innocenzi, Modulating the Optical Properties of Citrazinic Acid through the Monomer-to-Dimer Transformation, Journal of Physical Chemistry A. 124 (2020) 197–203. https://doi.org/10.1021/acs.jpca.9b10884.
[36] Y. Song, S. Zhu, S. Zhang, Y. Fu, L. Wang, X. Zhao, B. Yang, Investigation from chemical structure to photoluminescent mechanism: a type of carbon dots from the pyrolysis of citric acid and an amine, J Mater Chem C Mater. 3 (2015) 5976–5984. https://doi.org/10.1039/C5TC00813A.
[37] D. Qu, Z. Sun, The formation mechanism and fluorophores of carbon dots synthesized via a bottom-up route, Mater Chem Front. 4 (2020) 400–420. https://doi.org/10.1039/C9QM00552H.
[38] M. Langer, M. Paloncýová, M. Medved', M. Otyepka, Molecular Fluorophores Self-Organize into C-Dot Seeds and Incorporate into C-Dot Structures, J Phys Chem Lett. 11 (2020) 8252–8258. https://doi.org/10.1021/ACS.JPCLETT.0C01873.
[39] F. Siddique, M. Langer, M. Paloncýová, M. Medved', M. Otyepka, D. Nachtigallová, H. Lischka, A.J.A. Aquino, Conformational Behavior and Optical Properties of a Fluorophore Dimer as a Model of Luminescent Centers in Carbon Dots, The Journal of Physical Chemistry C. 124 (2020) 14327–14337. https://doi.org/10.1021/ACS.JPCC.0C02175.
[40] A. Cappai, C. Melis, L. Stagi, P.C. Ricci, F. Mocci, C.M. Carbonaro, Insight into the Molecular Model in Carbon Dots through Experimental and Theoretical Analysis of Citrazinic Acid in Aqueous Solution, Journal of Physical Chemistry C. 125 (2021) 4836–4845. https://doi.org/10.1021/acs.jpcc.0c10916.

[41] V. Strauss, J.T. Margraf, C. Dolle, B. Butz, T.J. Nacken, J. Walter, W. Bauer, W. Peukert, E. Spiecker, T. Clark, D.M. Guldi, Carbon Nanodots: Toward a Comprehensive Understanding of Their Photoluminescence, J Am Chem Soc. 136 (2014) 17308–17316. https://doi.org/10.1021/JA510183C.
[42] K. Hola, A.B. Bourlinos, O. Kozak, K. Berka, K.M. Siskova, M. Havrdova, J. Tucek, K. Safarova, M. Otyepka, E.P. Giannelis, R. Zboril, Photoluminescence effects of graphitic core size and surface functional groups in carbon dots: COO- induced red-shift emission, Carbon N Y. 70 (2014) 279–286. https://doi.org/10.1016/j.carbon.2014.01.008.
[43] Y. Li, H. Shu, X. Niu, J. Wang, Electronic and Optical Properties of Edge-Functionalized Graphene Quantum Dots and the Underlying Mechanism, Journal of Physical Chemistry C. 119 (2015) 24950–24957. https://doi.org/10.1021/acs.jpcc.5b05935.
[44] S. Chen, N. Ullah, R. Zhang, Engineering the excited state of graphitic carbon nitride nanostructures by covalently bonding with graphene quantum dots, Theor Chem Acc. 139 (2020) 9–14. https://doi.org/10.1007/s00214-019-2525-z.
[45] M. Gazzetto, A. Sciortino, M. Nazari, E. Rohwer, G. Giammona, N. Mauro, T. Feurer, F. Messina, A. Cannizzo, Photocycle of Excitons in Nitrogen-Rich Carbon Nanodots: Implications for Photocatalysis and Photovoltaics, ACS Appl Nano Mater. 3 (2020) 6925–6934. https://doi.org/10.1021/ACSANM.0C01259.
[46] H. Chen, G.D. Wang, X. Sun, T. Todd, F. Zhang, J. Xie, B. Shen, Mesoporous Silica as Nanoreactors to Prepare Gd-Encapsulated Carbon Dots of Controllable Sizes and Magnetic Properties, Adv Funct Mater. 26 (2016) 3973–3982. https://doi.org/10.1002/adfm.201504177.
[47] J. Zong, Y. Zhu, X. Yang, J. Shen, C. Li, Synthesis of photoluminescent carbogenic dots using mesoporous silica spheres as nanoreactors, Chemical Communications. 47 (2011) 764–766. https://doi.org/10.1039/c0cc03092a.
[48] K. Suzuki, L. Malfatti, M. Takahashi, D. Carboni, F. Messina, Y. Tokudome, M. Takemoto, P. Innocenzi, Design of Carbon Dots Photoluminescence through Organo-Functional Silane Grafting for Solid-State Emitting Devices, Sci Rep. 7 (2017) 1–11. https://doi.org/10.1038/s41598-017-05540-5.
[49] D. Fernandes, K.A. Heslop, A. Kelarakis, M.J. Krysmann, L. Estevez, In situ generation of carbon dots within a polymer matrix, Polymer (Guildf). 188 (2020) 122159. https://doi.org/10.1016/j.polymer.2020.122159.
[50] S. Mura, R. Ludmerczki, L. Stagi, S. Garroni, C.M. Carbonaro, P.C. Ricci, M.F. Casula, L. Malfatti, P. Innocenzi, Integrating sol-gel and carbon dots chemistry for the fabrication of fluorescent hybrid organic-inorganic films, Sci Rep. 10 (2020) 4770. https://doi.org/10.1038/s41598-020-61517-x.
[51] A. Madonia, M. Martin-Sabi, A. Sciortino, S. Agnello, M. Cannas, S. Ammar, F. Messina, D. Schaming, Highly Efficient Electron Transfer in a Carbon Dot–Polyoxometalate Nanohybrid, J Phys Chem Lett. 11 (2020) 4379–4384. https://doi.org/10.1021/ACS.JPCLETT.0C01078.
[52] J. Liu, N. Wang, Y. Yu, Y. Yan, H. Zhang, J. Li, J. Yu, Carbon dots in zeolites: A new class of thermally activated delayed fluorescence materials with ultralong lifetimes, Sci Adv. 3 (2017) e1603171. https://doi.org/10.1126/sciadv.1603171.
[53] J. Liu, H. Zhang, N. Wang, Y. Yu, Y. Cui, J. Li, J. Yu, Template-Modulated Afterglow of Carbon Dots in Zeolites: Room-Temperature Phosphorescence and Thermally Activated Delayed Fluorescence, ACS Mater Lett. 1 (2019) 58–63. https://doi.org/10.1021/acsmaterialslett.9b00073.

[54] Y. Ma, X. Zhang, J. Bai, K. Huang, L. Ren, Facile, controllable tune of blue shift or red shift of the fluorescence emission of solid-state carbon dots, Chemical Engineering Journal. 374 (2019) 787–792. https://doi.org/10.1016/j.cej.2019.06.016.
[55] J. Joseph, A.A. Anappara, Cool white, persistent room-temperature phosphorescence in carbon dots embedded in a silica gel matrix, Physical Chemistry Chemical Physics. 19 (2017) 15137–15144. https://doi.org/10.1039/c7cp02731a.
[56] A. Vassilakopoulou, V. Georgakilas, N. Vainos, I. Koutselas, Successful entrapment of carbon dots within flexible free-standing transparent mesoporous organic-inorganic silica hybrid films for photonic applications, Journal of Physics and Chemistry of Solids. 103 (2017) 190–196. https://doi.org/10.1016/j.jpcs.2016.12.027.
[57] Z. Guo, Z. Zhu, X. Zhang, Y. Chen, Facile synthesis of blue-emitting carbon dots@mesoporous silica composite spheres, Solid State Sci. 76 (2018) 100–104. https://doi.org/10.1016/j.solidstatesciences.2017.12.011.
[58] L. Sciortino, F. Messina, G. Buscarino, S. Agnello, M. Cannas, F.M. Gelardi, Nitrogen-doped carbon dots embedded in a SiO2 monolith for solid-state fluorescent detection of Cu2+ ions, Journal of Nanoparticle Research 2017 19:6. 19 (2017) 1–11. https://doi.org/10.1007/S11051-017-3915-6.
[59] Y. Liu, C.Y. Liu, Z.Y. Zhang, W.D. Yang, S.D. Nie, Plasmon-enhanced photoluminescence of carbon dots-silica hybrid mesoporous spheres, J Mater Chem C Mater. 3 (2015) 2881–2885. https://doi.org/10.1039/c4tc02599g.
[60] T. Sarkar, K. Rawat, P.R. Solanki, H.B. Bohidar, Carbon dots-embedded fluorescent silica xerogel, Colloids Surf A Physicochem Eng Asp. 583 (2019) 123844. https://doi.org/10.1016/j.colsurfa.2019.123844.
[61] A. Babusenan, B. Pandey, S.C. Roy, J. Bhattacharyya, Charge transfer mediated photoluminescence enhancement in carbon dots embedded in TiO2 nanotube matrix, Carbon N Y. 161 (2020) 535–541. https://doi.org/10.1016/j.carbon.2020.01.097.
[62] J. Li, B. Wang, H. Zhang, J. Yu, Carbon Dots-in-Matrix Boosting Intriguing Luminescence Properties and Applications, Small. 15 (2019) 1–16. https://doi.org/10.1002/smll.201805504.
[63] Y. Sun, J. Liu, X. Pang, X. Zhang, J. Zhuang, H. Zhang, C. Hu, M. Zheng, B. Lei, Y. Liu, Temperature-responsive conversion of thermally activated delayed fluorescence and room-temperature phosphorescence of carbon dots in silica, J Mater Chem C Mater. 8 (2020) 5744–5751. https://doi.org/10.1039/d0tc00507j.
[64] Y. Sun, S. Liu, L. Sun, S. Wu, G. Hu, X. Pang, A.T. Smith, C. Hu, S. Zeng, W. Wang, Y. Liu, M. Zheng, Ultralong lifetime and efficient room temperature phosphorescent carbon dots through multi-confinement structure design, Nat Commun. 11 (2020) 1–11. https://doi.org/10.1038/s41467-020-19422-4.
[65] C.M. Carbonaro, S.V. Thakkar, R. Ludmerczki, C. Olla, A. Pinna, D. Loche, L. Malfatti, F. Cesare Marincola, M.F. Casula, How porosity affects the emission of fluorescent carbon dot-silica porous composites, Microporous and Mesoporous Materials. 305 (2020). https://doi.org/10.1016/j.micromeso.2020.110302.
[66] C.M. Carbonaro, P.C. Ricci, S. Grandi, M. Marceddu, R. Corpino, M. Salis, A. Anedda, On the formation of aggregates in silica-rhodamine 6G type II hybrids, RSC Adv. 2 (2012) 1905–1912. https://doi.org/10.1039/c2ra00830k.
[67] C.M. Carbonaro, F. Meinardi, P.C. Ricci, M. Salis, A. Anedda, Light assisted dimer to monomer transformation in heavily doped rhodamine 6G-porous silica hybrids, Journal of Physical Chemistry B. 113 (2009) 5111–5116. https://doi.org/10.1021/jp810835j.
[68] N.M. Zholobak, A.L. Popov, A.B. Shcherbakov, N.R. Popova, M.M. Guzyk, V.P. Antonovich, A. V. Yegorova, Y. V. Scrypynets, I.I. Leonenko, A.Y. Baranchikov, V.K. Ivanov, Facile fabrication of luminescent organic dots by thermolysis of citric acid in urea melt, and their use for cell staining and polyelectrolyte microcapsule

labelling, Beilstein Journal of Nanotechnology. 7 (2016) 1905–1917. https://doi.org/10.3762/BJNANO.7.182.
[69] P. Fermo, M. Andreoli, L. Bonizzoni, M. Fantauzzi, G. Giubertoni, N. Ludwig, A. Rossi, Characterisation of Roman and Byzantine glasses from the surroundings of Thugga (Tunisia): Raw materials and colours, Microchemical Journal. 129 (2016) 5–15. https://doi.org/10.1016/J.MICROC.2016.05.014.
[70] J.R. Lakowicz, Principles of Fluorescence Spectroscopy, Springer US, Boston, MA, 2006. https://doi.org/10.1007/978-0-387-46312-4.
[71] M.J. Frisch, G.W. Trucks, H.B. Schlegel, G.E. Scuseria, M. a. Robb, J.R. Cheeseman, G. Scalmani, V. Barone, G. a. Petersson, H. Nakatsuji, X. Li, M. Caricato, a. V. Marenich, J. Bloino, B.G. Janesko, R. Gomperts, B. Mennucci, H.P. Hratchian, J. V. Ortiz, a. F. Izmaylov, J.L. Sonnenberg, Williams, F. Ding, F. Lipparini, F. Egidi, J. Goings, B. Peng, A. Petrone, T. Henderson, D. Ranasinghe, V.G. Zakrzewski, J. Gao, N. Rega, G. Zheng, W. Liang, M. Hada, M. Ehara, K. Toyota, R. Fukuda, J. Hasegawa, M. Ishida, T. Nakajima, Y. Honda, O. Kitao, H. Nakai, T. Vreven, K. Throssell, J. a. Montgomery Jr., J.E. Peralta, F. Ogliaro, M.J. Bearpark, J.J. Heyd, E.N. Brothers, K.N. Kudin, V.N. Staroverov, T. a. Keith, R. Kobayashi, J. Normand, K. Raghavachari, a. P. Rendell, J.C. Burant, S.S. Iyengar, J. Tomasi, M. Cossi, J.M. Millam, M. Klene, C. Adamo, R. Cammi, J.W. Ochterski, R.L. Martin, K. Morokuma, O. Farkas, J.B. Foresman, D.J. Fox, G16_C01, (2016) Gaussian 16, Gaussian, Inc., Wallin.
[72] Atsuko Aboshi, and Naoko Kurumoto, T. Yamada, T. Uchino*, Influence of Thermal Treatments on the Photoluminescence Characteristics of Nanometer-Sized Amorphous Silica Particles, Journal of Physical Chemistry C. 111 (2007) 8483–8488. https://doi.org/10.1021/JP0718505.
[73] C.M. Carbonaro, M. Salis, R. Corpino, D. Chiriu, L. Stagi, G. Serra, A. Bosin, P.C. Ricci, Thermodynamic models of the adsorption and desorption of molecular oxygen at the UV and blue emitting centers in mesoporous silica under variable oxygen pressure, Microporous and Mesoporous Materials. 239 (2017) 371–380. https://doi.org/10.1016/j.micromeso.2016.10.037.
[74] F. Mocci, C. Olla, A. Cappai, R. Corpino, P.C. Ricci, D. Chiriu, M. Salis, C.M. Carbonaro, Formation of Citrazinic Acid Ions and Their Contribution to Optical and Magnetic Features of Carbon Nanodots: A Combined Experimental and Computational Approach, Materials. 14 (2021) 770. https://doi.org/10.3390/ma14040770.
[75] X. Shao, A.J.A. Aquino, M. Otyepka, D. Nachtigallová, H. Lischka, Tuning the UV spectrum of PAHs by means of different N-doping types taking pyrene as paradigmatic example: Categorization: Via valence bond theory and high-level computational approaches, Physical Chemistry Chemical Physics. 22 (2020) 22003–22015. https://doi.org/10.1039/d0cp02688c.
[76] A.D. Becke, A. D., Density-functional thermochemistry. III. The role of exact exchange, JChPh. 98 (1993) 5648–5652. https://doi.org/10.1063/1.464913.
[77] J. Tirado-Rives, W.L. Jorgensen, Performance of B3LYP density functional methods for a large set of organic molecules, J Chem Theory Comput. 4 (2008) 297–306. https://doi.org/10.1021/ct700248k.
[78] A. Anedda, C.M. Carbonaro, F. Clemente, R. Corpino, F. Raga, A. Serpi, Ultraviolet excitation of photoluminescence of porous silica under vacuum conditions, J Non Cryst Solids. 322 (2003) 95–99. https://doi.org/10.1016/S0022-3093(03)00184-4.
[79] A. Anedda, C.M. Carbonaro, F. Clemente, R. Corpino, S. Grandi, OH-dependence of ultraviolet emission in porous silica, 322 (2003) 68–72. https://doi.org/10.1016/S0022-3093(03)00176-5.

[80] J.-R. Macairan, T. v. de Medeiros, M. Gazzetto, F. Yarur Villanueva, A. Cannizzo, R. Naccache, Elucidating the mechanism of dual-fluorescence in carbon dots, J Colloid Interface Sci. 606 (2022) 67–76. https://doi.org/10.1016/j.jcis.2021.07.156.
[81] Y. He, J. He, L. Wang, Z. Yu, H. Zhang, Y. Liu, B. Lei, Synthesis of double carbon dots co-doped mesoporous Al2O3 for ratiometric fluorescent determination of oxygen, Sens Actuators B Chem. 251 (2017) 918–926. https://doi.org/10.1016/j.snb.2017.05.104.
[82] A. Terracina, A. Armano, M. Meloni, A. Panniello, G. Minervini, A. Madonia, M. Cannas, M. Striccoli, L. Malfatti, F. Messina, Photobleaching and Recovery Kinetics of a Palette of Carbon Nanodots Probed by In Situ Optical Spectroscopy, ACS Appl Mater Interfaces. (2022). https://doi.org/10.1021/acsami.2c09496.
[83] M. Sun, C. Liang, Z. Tian, E. V. Ushakova, D. Li, G. Xing, S. Qu, A.L. Rogach, Realization of the Photostable Intrinsic Core Emission from Carbon Dots through Surface Deoxidation by Ultraviolet Irradiation, J Phys Chem Lett. 10 (2019) 3094–3100. https://doi.org/10.1021/acs.jpclett.9b00842.
[84] G. Minervini, A. Panniello, A. Madonia, C.M. Carbonaro, F. Mocci, T. Sibillano, C. Giannini, R. Comparelli, C. Ingrosso, N. Depalo, E. Fanizza, M.L. Curri, M. Striccoli, Photostable carbon dots with intense green emission in an open reactor synthesis, Carbon N Y. 198 (2022) 230–243. https://doi.org/10.1016/j.carbon.2022.07.034.
[85] S. Sarkar, J. Chowdhury, S. Dutta, T. Pal, A pH dependent Raman and surface enhanced Raman spectroscopic studies of citrazinic acid aided by theoretical calculations, Spectrochim Acta A Mol Biomol Spectrosc. 169 (2016) 108–115. https://doi.org/10.1016/J.SAA.2016.06.023.
[86] N. V. Bashmakova, Y.O. Shaydyuk, A.M. Dmytruk, T. Świergosz, O.D. Kachkovsky, K.D. Belfield, M. V. Bondar, W. Kasprzyk, Nature of linear spectral properties and fast electronic relaxations in green fluorescent pyrrolo[3,4-c]pyridine derivative, Int J Mol Sci. 22 (2021). https://doi.org/10.3390/ijms22115592.
[87] C.M. Carbonaro, Tuning the formation of aggregates in silica–Rhodamine 6G hybrids by thermal treatment, J Photochem Photobiol A Chem. 222 (2011) 56–63. https://doi.org/10.1016/J.JPHOTOCHEM.2011.05.001.
[88] A. Anedda, C.M. Carbonaro, F. Clemente, L. Corda, R. Corpino, P.C. Ricci, Surface hydroxyls in porous silica: a Raman spectroscopy study, Materials Science and Engineering: C. 23 (2003) 1069–1072. https://doi.org/10.1016/j.msec.2003.09.125.
[89] J. Wang, Y. Yang, X. Liu, Solid-state fluorescent carbon dots: quenching resistance strategies, high quantum efficiency control, multicolor tuning, and applications, Mater Adv. 1 (2020) 3122–3142. https://doi.org/10.1039/D0MA00632G.
[90] C.M. Carbonaro, F. Orrù, P.C. Ricci, A. Ardu, R. Corpino, D. Chiriu, F. Angius, A. Mura, C. Cannas, High efficient fluorescent stable colloidal sealed dye-doped mesostructured silica nanoparticles, Microporous and Mesoporous Materials. 225 (2016) 432–439. https://doi.org/10.1016/j.micromeso.2016.01.028.

Chiara Olla, Pier Carlo Ricci, Daniele Chiriu, Marzia Fantauzzi, Maria Francesca Casula, Francesca Mocci, Antonio Cappai, Stefania Porcu, Luigi Stagi, Carlo Maria Carbonaro**

Selecting molecular or surface centers in Carbon Dots-silica hybrids to tune the optical emission: a photo-physics study down to the atomistic level

Synthesis of Carbon Dots in mesoporous silica produces solid-state hybrids with a larger content of graphitic N and imidic groups, lower content of pyridinic N, and a composite emission with a larger contribution in the green range, as compared to CDs synthesized outside silica. Different emitting centers are identified in the two systems, mostly molecular centers in CDs dispersed in water and mostly surface centers in CD-silica hybrids. Photo-physics analysis enlightens the active role of silica matrix in tuning size and emission properties and blue-to-green photo-activated reaction mechanisms.

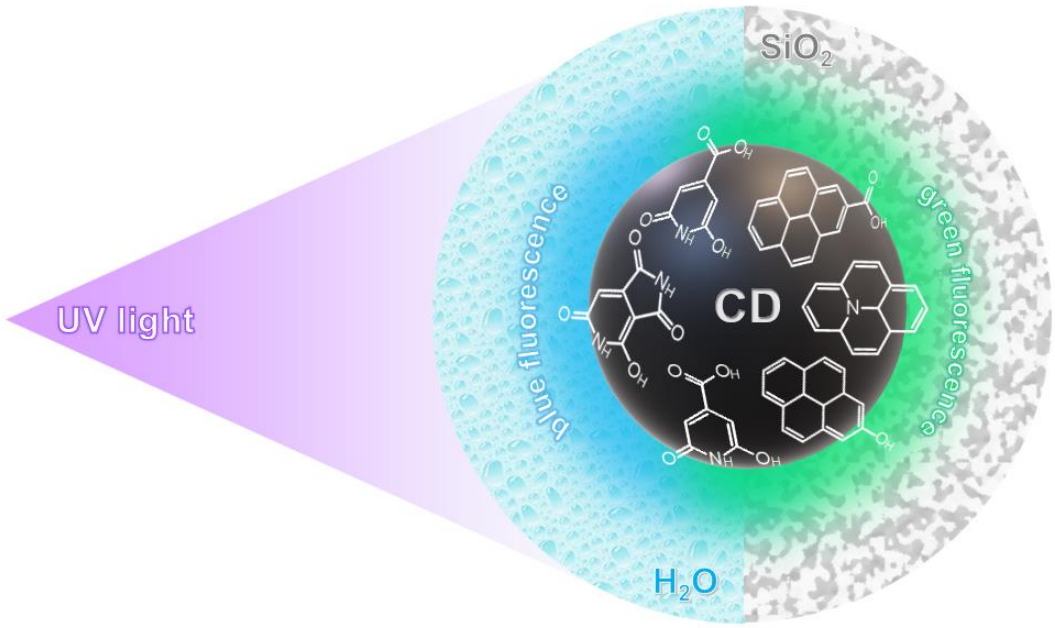

Supporting Information

Selecting molecular or surface centers in Carbon Dots-silica hybrids to tune the optical emission: a photo-physics study down to the atomistic level

Chiara Olla, Pier Carlo Ricci, Daniele Chiriu, Marzia Fantauzzi, Maria Francesca Casula, Francesca Mocci, Antonio Cappai, Stefania Porcu, Luigi Stagi, Carlo Maria Carbonaro**

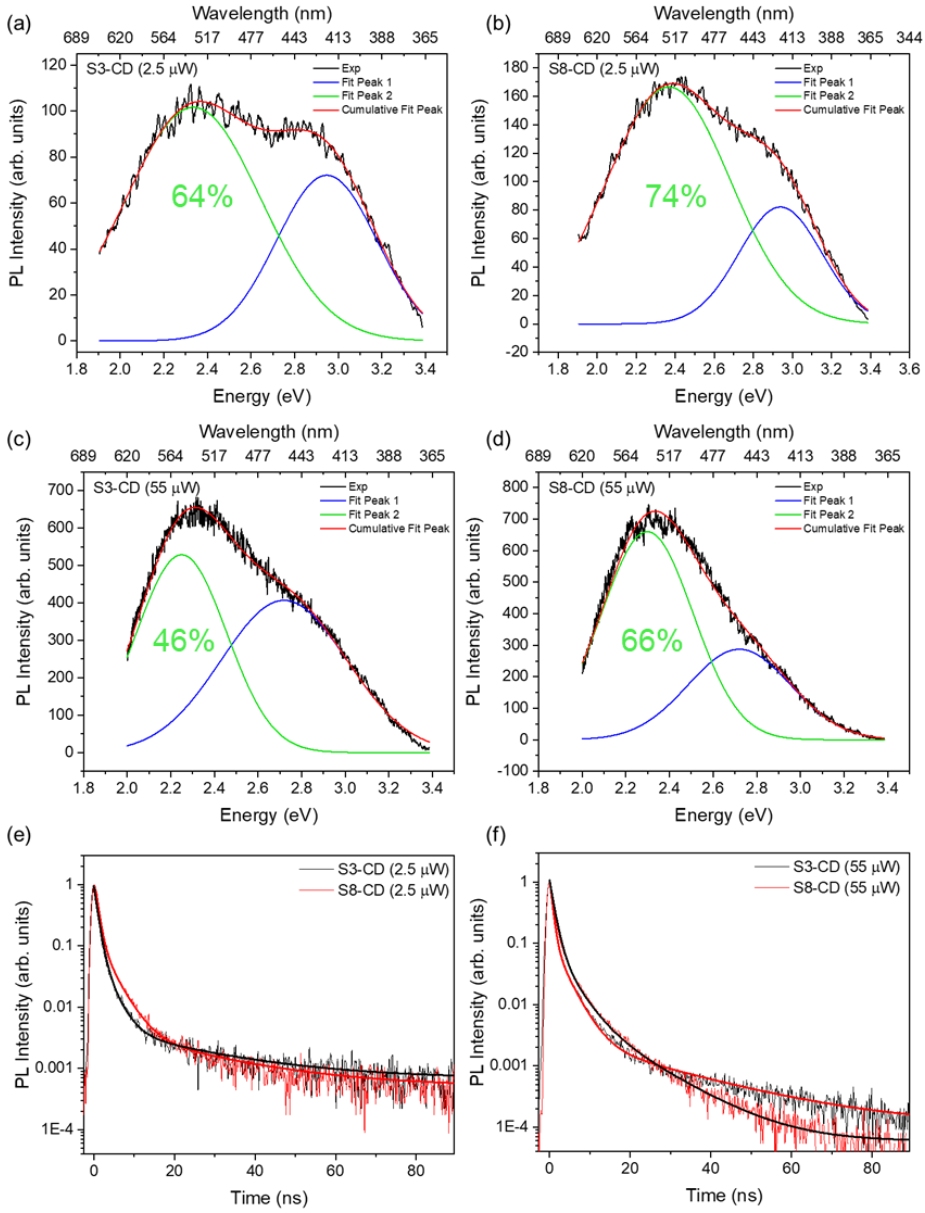

Figure S1. Gaussian deconvolution of hybrid samples irradiated at 350 nm at low (2.5 µW) and high (55 µW) excitation power and corresponding decay time plots with relative fits (details in Table S1 and S2). Jacobian factor for the correction of the PL intensity was applied in all spectra.

Table S1: Gaussian band deconvolution data of S3-CD, S8-CD hybrids, and CD-R sample excited at 350 nm.

	Peak 1 (eV-nm)	FWHM (eV)	Relative Area (%)	Peak 2 (eV-nm)	FWHM (eV)	Relative Area (%)
S3-CD@350nm (2.5uW)	2.95 - 421	0.54	35.8	2.34 - 531	0.74	64.2
S3-CD@350nm (55uW)	2.72 - 456	0.68	54.4	2.25 - 551	0.49	45.6
S8-CD@350nm (2.5uW)	2.94 - 422	0.50	26.0	2.37 - 524	0.74	74.0
S8-CD@350nm (55uW)	2.72 - 456	0.55	34.5	2.30 - 539	0.49	65.5
CD-R@350nm (2.5-55 uW)	2.82 - 440	0.54	73.0	2.46 - 503	0.71	27.0

Table S2: Exponential deconvolution of decay time data of S3-CD, S8-CD hybrids, and CD-R sample excited at 350 nm.

	A_1	τ_1 (ns)	A_2	τ_2 (ns)	A_3	τ_3 (ns)	τ_{mean} (ns)
S3-CD@350nm(2.5uW)	119645	0.61	1620	2.81	37	21.66	0.95
S3-CD@350nm(55uW)	24350	0.56	5892	2.56	370	11.35	2.85
S8-CD@350nm(2.5uW)	13563	0.79	1747	3.25	59	16.93	2.52
S8-CD@350nm(55uW)	30310	0.69	6038	2.58	980	7.85	2.60
CD-R@350nm (2.5-55 uW)	1089	0.32	1411	2.08	982	9.21	7.26

The average lifetime was calculated as the weighted mean of the retrieved values (J.R. Lakowicz, Principles of Fluorescence Spectroscopy, Springer US, Boston, MA, 2006. https://doi.org/10.1007/978-0-387-46312-4):

$$\bar{\tau} = \sum_{i=1}^{n} \frac{\alpha_i \tau_i^2}{\alpha_i \tau_i}$$

Table S3. Elemental composition in percentage (%) from XPS data (th = theoretical).

	C_{tot}	O_{tot}	N_{tot}	Tot	C/O (0.8 th.)	C/N (3.4 th.)
CD-R	67	21	12	100	3.2	5.6
S3-CD (w/o SiO_2)	52	38	10	100	1.4	5.2
S8-CD (w/o SiO_2)	64	22	14	100	2.9	4.6

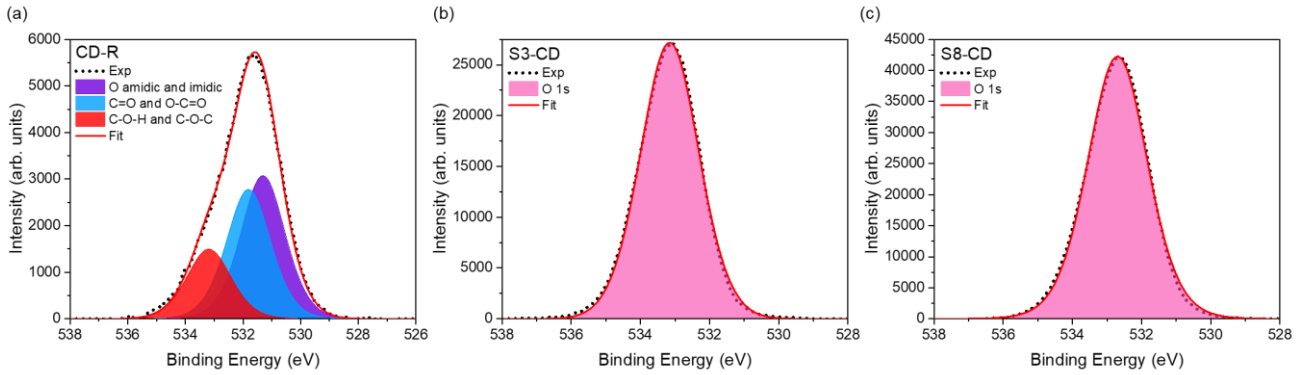

Figure S2. O1s XPS spectra of CD-R (a), S3-CD (b) and S8-CD (c).

Table S4. Data in percentage (%) from XPS O_{1s} spectra.

	C=O O-C=O	C-O-H C-O-C	O_{1s}	$O_{amidic/imidic}$
CD-R	37.83	20.29	-	41.88
S3-CD (w/o SiO2)	-	-	100	-
S8-CD (w/o SiO2)	-	-	100	-

Table S5. Data in percentage (%) from XPS C_{1s} spectra.

	$C_{graphitic}$	$C_{aromatic}$	$C_{aliphatic}$	C-O/C-N	COO- O=C-N	COOH	C_{org}/C_{graph}
CD-R	2.74	27.37	28.14	14.30	24.65	2.80	35.5
S3-CD (w/o SiO2)	3.41	2.05	31.74	26.15	15.25	21.41	28.3
S8-CD (w/o SiO2)	1.52	5.73	32.28	22.25	18.29	19.92	64.4

Table S6 Data in percentage (%) from XPS N_{1s} spectra.

	$N_{pyridinic/amines}$	$N_{pyrrolic}$	$N_{graphitic}$	N-C=O (N_{imidic})
CD-R	18.36	73.98	1.99	5.67
S3-CD (w/o SiO_2)	1.75	39.48	14.37	44.40
S8-CD (w/o SiO_2)	1.89	70.72	10.82	16.57

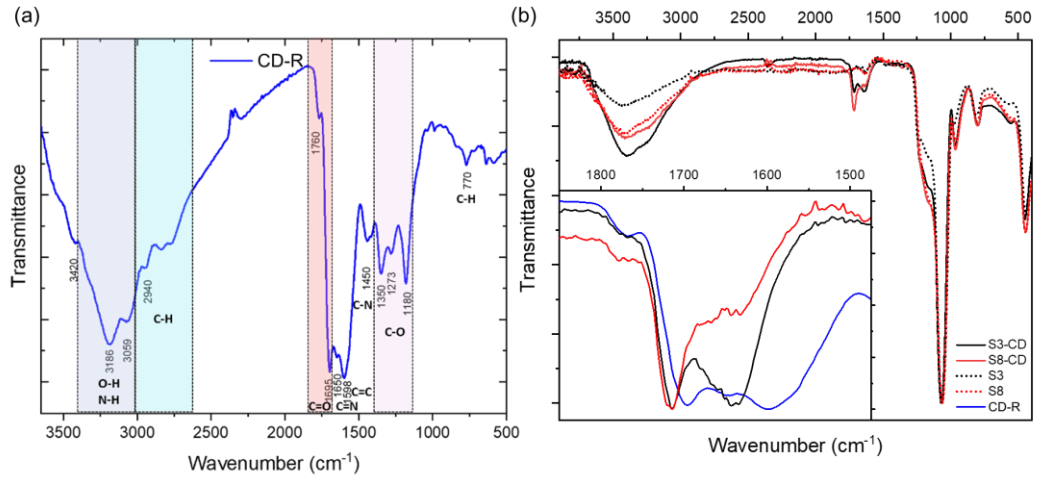

Figure S3. ATR spectra of (a) CD-R reference and (b) silica and silica hybrids with a comparison with CD-R in the insight.

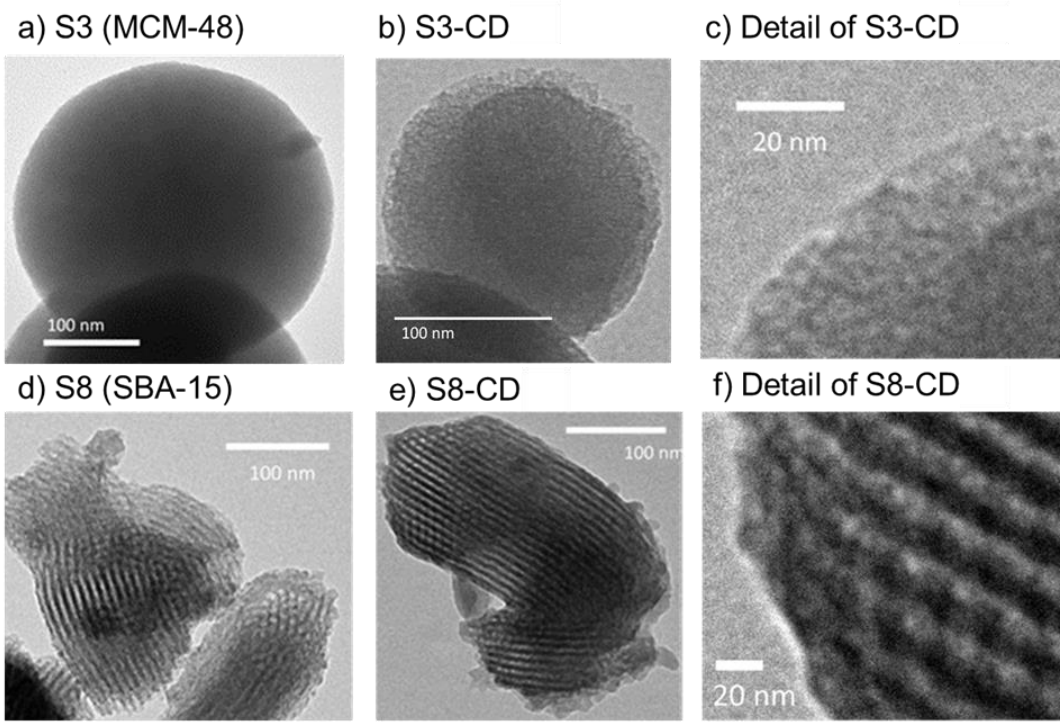

Figure S4. TEM images of void silica matrices (a,d) and silica-CD hybrids (b,c,e,f).

Figure S5. N_2 adsorption–desorption curves at 77 K of S3-CD (black line) and S3 (green line) samples (a), S8-CD (red line) and S8 (purple line) samples (b).

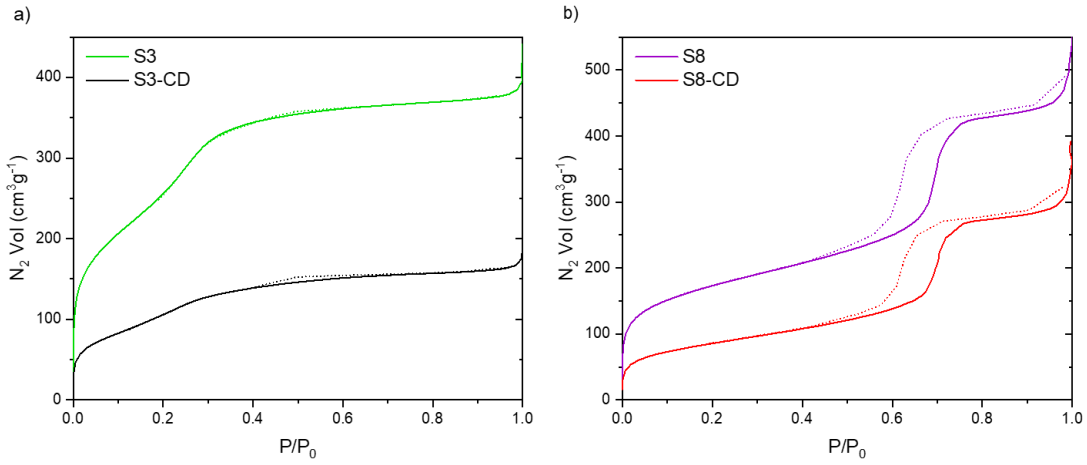

Table S7 Surface area and pore volume of silica matrices and S-CD hybrids.

	S3	**S3-CD**	**S8**	**S8-CD**
S_{BET} ($m^2 \cdot g^{-1}$)	984	418	610	308
V_P ($cm^3 \cdot g^{-1}$)	0,59	0,27	0,81	0,54

Table S8 QY of the reference sample and the CDs extracted from the hybrids.

	QY (λ_{exc} = 350 nm)	**QY (λ_{exc} = 440 nm)**
CD-R	4.7 %	6.5 %
CD-3	4.0 %	5.4 %
CD-8	4.4 %	5.2 %

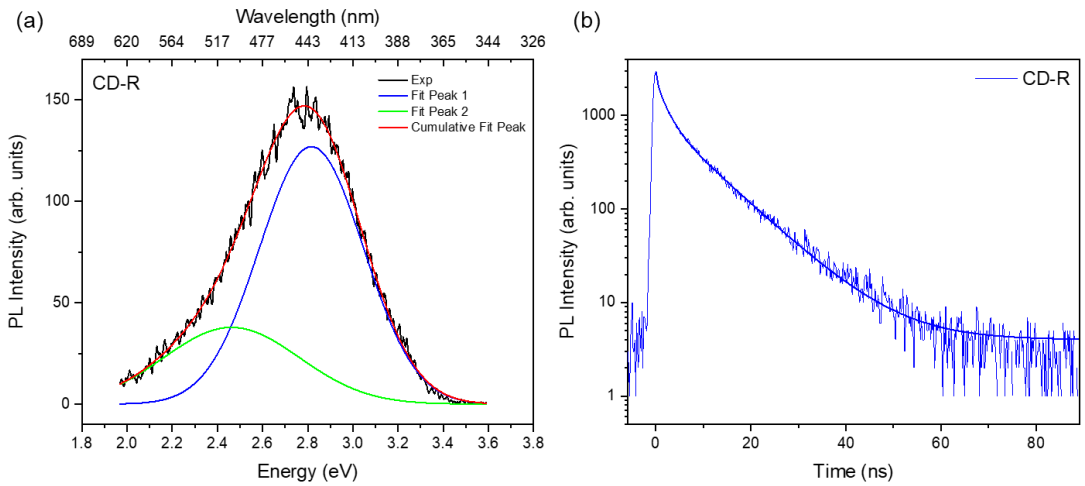

Figure S6: Spectral deconvolution by gaussian bands of CD-R sample (a) and data fit of its decay time (b) excited at 350 nm. Details in Table S1 and S2.

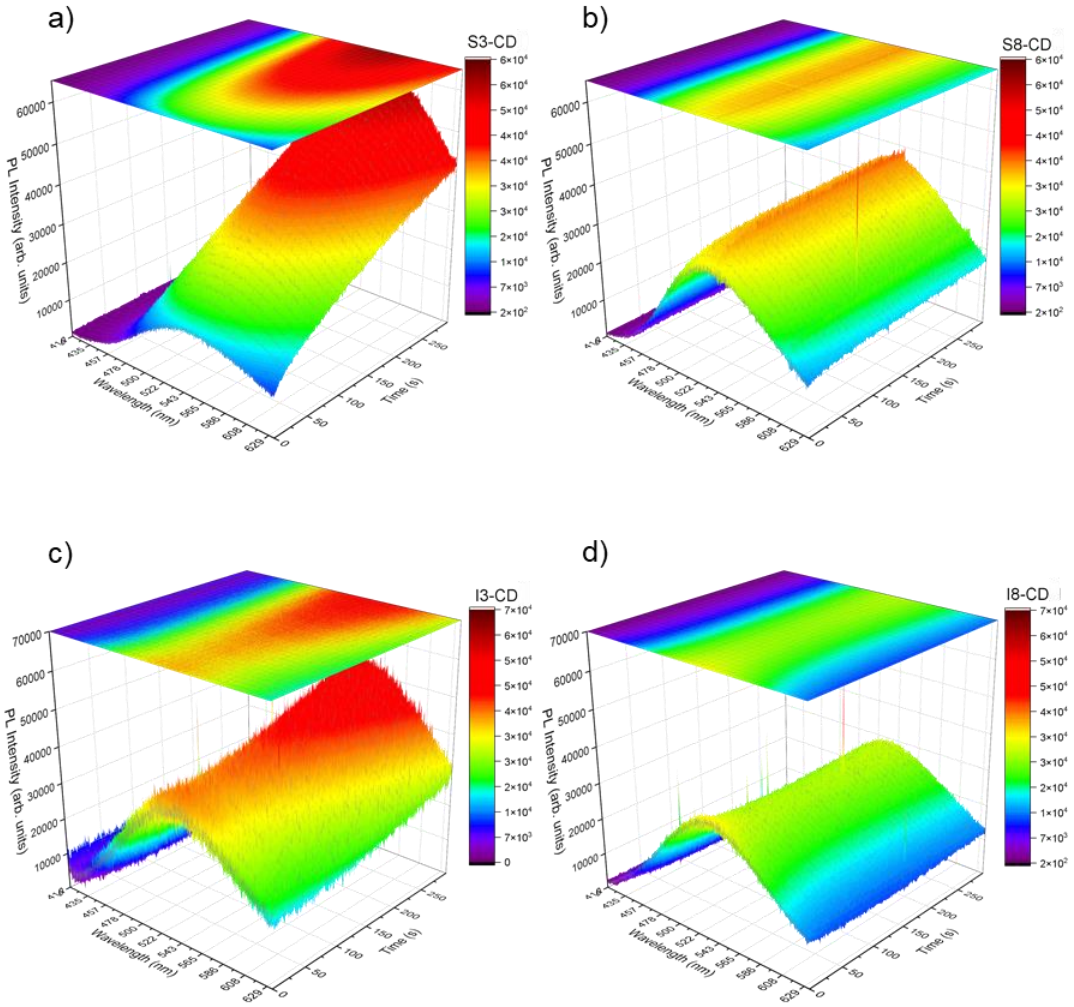

Figure S7. 3D plots of irradiation effects on S3-CD (a) and S8-CD (b), I3-CD (c), I8-CD (d). Laser irradiation was performed with 405 nm CW light focused on the samples with a microscope objective (power 5 μW, spot diameter 6.4 μm).

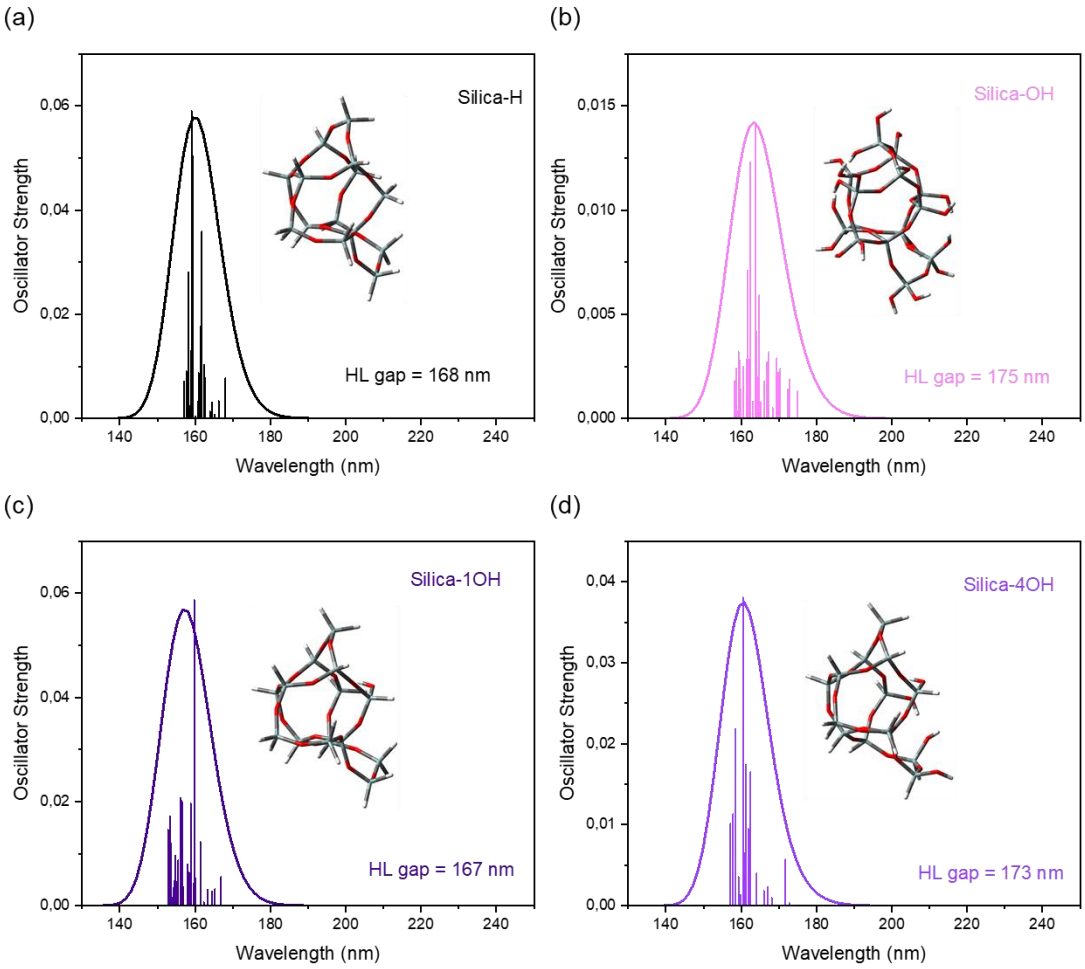

Figure S8: Calculated optical absorption features of isolated emitting center models (simplified stick representation: white stick = H atom, dark grey stick = C atom, red stick = O atom).

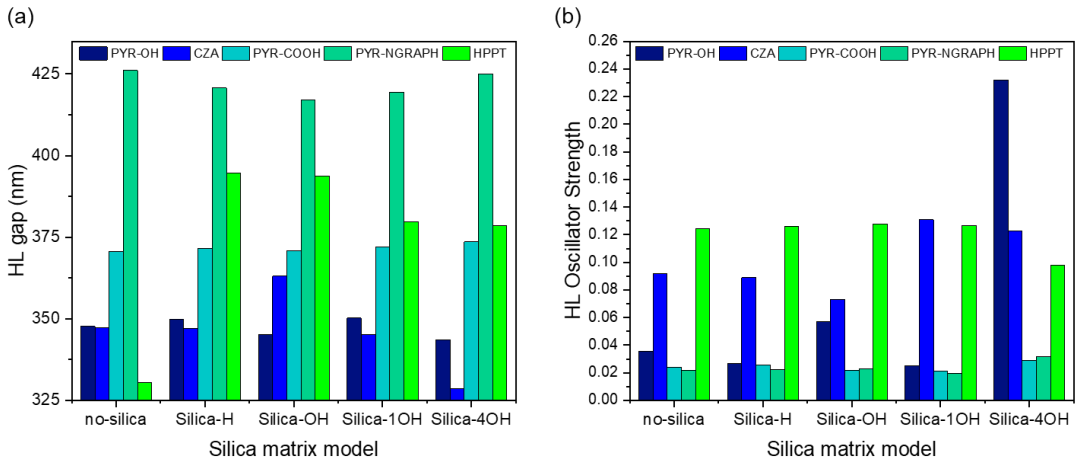

Figure S9: HL gap (left) and oscillator strength (right) for the different model structures without silica, or in presence of fully H terminated, fully OH terminated silica, and partially OH terminated (1 OH or 4 OH) silica models.